UNIVERSITY OF CAPE COAST

MULTISPECTRAL IMAGING OF PLASMODIUM FALCIPARUM INFECTED AND UNINFECTED SICKLE DISEASE AND SICKLE TRAIT RED BLOOD CELLS

NANA ESI NYARKO

2021

UNIVERSITY OF CAPE COAST

MULTISPECTRAL IMAGING OF PLASMODIUM FALCIPARUM INFECTED AND UNINFECTED SICKLE DISEASE AND SICKLE TRAIT RED BLOOD CELLS

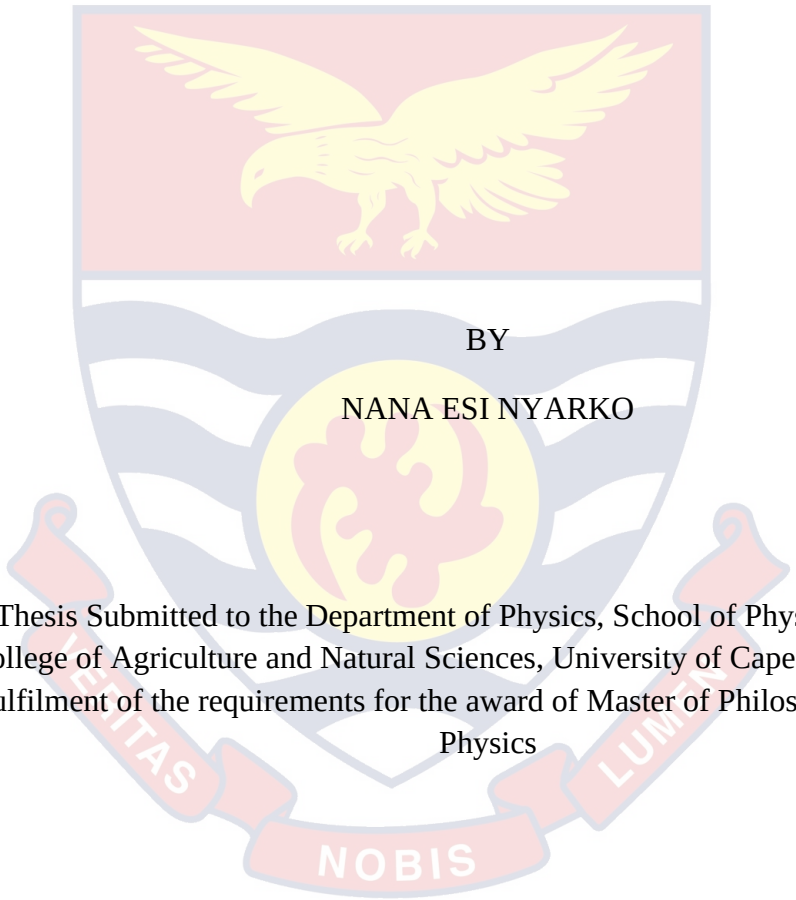

BY

NANA ESI NYARKO

Thesis Submitted to the Department of Physics, School of Physical Sciences, College of Agriculture and Natural Sciences, University of Cape Coast, in partial fulfilment of the requirements for the award of Master of Philosophy Degree in Physics

JULY 2021

DECLARATION

Candidate's Declaration

I hereby declare that this thesis is the result of my own original work and that no part of it has been presented for another degree in this University or elsewhere.

Candidate's Signature: …….. Date: ……

Name: Nana Esi Nyarko

Supervisors' Declaration

We hereby declare that the preparation and presentation of the thesis were supervised in accordance with the guidelines on supervision of thesis laid down by the University of Cape Coast.

Principal Supervisors' Signature: …… Date: ……

Name: Prof. Moses J. Eghan

Co-Supervisors' Signature: …… Date: ……

Name: Prof. Benjamin Anderson

ABSTRACT

In this work, multispectral imaging technique was used to discriminate between *Plasmodium falciparum* infected sickle red blood cells (SIRBCs) (sickle cell trait (AS) (AS-IRBCs) and sickle cell disease (SS) (SS-IRBCs)) and their respective uninfected sickle red blood cells (SURBCs) (AS-URBCs, SS-URBCs)). Giemsa stained blood smear slides were prepared from cultured samples of AS-IRBCs, AS-URBCs, SS-IRBCs and SS-URBCs that have been kept for one (D1) and six days (D6). Optical characteristics of SIRBCs and SURBCs in transmission mode showed a general increase in transmitted light intensities for SIRBCs and decreased in transmitted light intensities for URBCs for most of the thirteen (13) excitation wavelengths employed. Principal component analysis revealed 700 nm wavelength as a standard marker for discriminating between SIRBCs and SURBCs for both AS and SS. Other wavelengths (435 nm, 700 nm, and 810 nm) were common markers for AS-IRBCs-D1 and AS-IRBCs-D6 with the 750 nm being a unique marker for AS-IRBCsD6. Whereas 590 nm, 700 nm and 750 nm were found as markers for discriminating between SIRBCs and SURBCs of SS- IRBCs-D1 and SS- IRBCs-D6, 435 nm and 810 nm were unique markers for SS- IRBCs D6 only. This multispectral imaging technique can be envisioned as a tool for diagnosing sickle cell anaemia patients infected with malaria.

KEY WORDS

Culture

Malaria Parasite

Multispectral Imaging Microscopic Technique

Red Blood Cells

Sickle Cell Disease

Transmission

ACKNOWLEDGEMENTS

This thesis would not have come to successful completion without the support of numerous people who have contributed in diverse ways. First and foremost, I would like to express my profound gratitude to Prof. Moses Jojo Eghan my principal supervisor and Dr Benjamin Anderson my co-supervisor for their tremendous supervision, advice and guidance from the early stage of this research and throughout the work. Many thanks to all lecturers at the Laser and Fibre Optic Centre (LAFOC). I am grateful for the opportunity to develop as a researcher under their tutelage.

My sincere gratitude also goes to Dr Michael Fokuo Ofori, the director of immunology, Dr Asamoah Kusi and Miss Belinda Aculley at the Noguchi Memorial Research Center. I am not forgetting Dr Akwaasi Ayamful. A special thanks to all my friends and colleagues in our group, especially Dr Charles Loyd-Yeboah Amuah, Dr Jerry Opoku-Ansah, Dr Peter Osei-Wusu Adueming, Mr. Rabbi Boateng, Mr Calvin Gaffrey, Mr. Andrew Huzortey and Mr Barnabas Graves. I am also grateful to the entire administrative staff of LAFOC for all the fantastic discussions that we had about religion, politics, sports and life.

My dad Prof. Benjamin Kofi Nyarko, deserves a special mention for his inseparable financial and emotional support. I am incredibly grateful for his patience and help he offered me throughout this period, and Mrs Jemimah Assabil, my mom, for her prayers and encouragement. Pardon me if your name was not mentioned.

DEDICATION

To all the members of the Nyarko Family and my Grandparents.

TABLE OF CONTENTS

LIST OF TABLES

LIST OF FIGURES

LIST OF ABBREVIATIONS

ACD	Acid Citrate Dextrose
ACS	Acute Chest Syndrome
AA-IRBC-D1	AA Infected Red Blood Cells Day 1
AA-IRBC-D6	AA Infected Red Blood Cells Day 6
AA-URBC	AA Uninfected Red Blood Cells
AS-IRBC-D1	AS Infected Red Blood Cells Day 1
AS-IRBC-D6	AS Infected Red Blood Cells Day 6
AS-URBC	AS Uninfected Red Blood Cells
BSC	Biosafety Cabinet
CA	Correspondence Analysis
CCD	Charge-Coupled Device
CCTH	Cape Coast Teaching Hospital
CPM	Complete Parasite Medium
DNA	Deoxyribonucleic Acid
EM	Electromagnetic
FIR	Far Infrared
HPLC	High Performance Liquid Chromatography
IRBC	Infected Red Blood Cells
LED	Light Emitting Diode
LIF	Laser-Induced Fluorescence
MATLAB	Matrix Laboratory
MCA	Multiple Correspondence Analysis
MDS	Multidimensional Scaling
MLR	Multiple Linear Regression
MSIM	Multispectral Imaging Microscope
MSLEDIM	Multispectral Light Emitting Diode Imaging Microscope
NMIMR	Noguchi Memorial Institute For Medical Research
PCA	Principal Component Analysis
PCR	Principal Component Regression
PLSR	Partial Least Square Regression
PWM	Parasite Wash Medium

QBC	Quantitative Buffy Coat
RBC	Red Blood Cells
RGB	Red Green and Blue
RR	Ridge Regression
SCA	Sickle Cell Anaemia
SCD	Sickle Cell Disease
SIRBCs	Sickle Infected Red Blood Cells
SURBCs	Sickle Uninfected Red Blood Cells
SS-IRBC-D1	SS Infected Red Blood Cells Day 1
SS-IRBC-D6	SS Infected Red Blood Cells Day 6
SS-URBC	SS Uninfected Red Blood Cells
UV	Ultra-Violet
URBC	Uninfected Red Blood cells
WHO	World Health Organization

CHAPTER ONE

INTRODUCTION

Background to the Study

Sickle cell disease refers to a group of inherited genetic disorders of the red blood cells (Kanchanawong, 2017). At low oxygen tension, red blood cells tend to become sickle-shaped and block the flow of blood cells. The deformed cells cause multiple organ failure by hindering the distribution of oxygen by red blood cells to other parts of the body. The ability of the genetic disorders of sickle cell disease to exhibit themselves in different ways makes the condition complicated. The disease has much diversity of phenotypes such as cardiac complication, pain episodes and hematological complications (Ballas, Lieff, Benjamin, & Dampier, 2010; T. N. Williams & Thein, 2018). Some sickle cell patients experience a different range of health complications whiles others experience few to no symptoms. The complication of the disease varies for each patient; some pass-on during their childhood whiles others during old age (Wilkie & Werley, 2013).

According to the World Health Organization (WHO), each year about three hundred thousand (300,000) children in Africa are born with significant haemoglobin disorders counting more than two hundred thousand (200,000) cases of sickle-cell anaemia. It is estimated by WHO that in Africa, 70 % of deaths caused by sickle cell anaemia (SCA) are preventable with simple, cost effective mediation like early identification of SCA patients by newborn screening (NBS) and the subsequent provision of comprehensive care (W.H.O, 2018). Extensive care involves immediate treatment and protection from infections, with

oral penicillin and vaccination against Streptococcus pneumonia. There is a significant mortality reduction in countries that make use of these interventions (Makani et al., 2011).

The sickle cell gene is well known in Africa due to the resistance it confers to plasmodium falciparum during a critical period of early childhood, favouring the survival of the host and subsequent transmission of the abnormal haemoglobin gene. A major determinant of morbidity and mortality of sickle cell trait is its ability to achieve a survival advantage in malarial areas (Indies, 2019). The interaction of malaria with sickle cell disease is likely to change the characteristics of the disease and shed serious doubt on the relevance of interventions developed in non-malarial areas (Indies, 2019)..

Diagnosis of malaria is made based on the patient's symptoms and signs such as fever, headache, chills, dizziness, diarrhoea, anorexia, nausea and many more. All these symptoms are used to identify the early stages of malaria. Conventional clinical diagnosis of malaria such as a microscopic diagnosis by staining thin blood smears, Quantitative Buffy Coat (QBC method), Rapid Diagnostic Test (Para Hit, Para Screen, SD Bioline), and Routine Diagnostic Test (RDT) can be used to determine any stage of malaria (Tangpukdee, Duangdee, Wilairatana, & Krudsood, 2009).

Conventional clinical diagnosis of malaria is made by microscopic examination of stained blood films with Giemsa, Wright's or Field's stain. This is done by staining thick and thin blood films on a glass slide (Warhurst & William, 1996). The tip of a patient's finger is sterilized by rubbing 70 % alcohol and allowing it to dry for 20 seconds and then the fingertip is pricked with a sharp,

sterile blood lancet and two to three droplets of blood are placed on the slide. A thin or thick blood smear is made from the droplet of blood and is allowed to dry for three (3) mins. After drying, the slide of blood is stained with a diluted Giemsa and washed in buffered water for three mins, and the slide is allowed to dry in a vertical position before it is examined under a light microscope (Chotivanich, Silamut, & Day, 2007). Nonetheless, the microscopic examination has its shortcoming. The staining and interpreting process requires trained and expert medical personnel, especially in the identification of parasite at low parasitaemia (Payne, 1988).

Quantitative buffy coat (QBC) method is used in the simplification of malaria diagnosis by enhancing the microscopic detection of the parasite. This method requires staining the parasite deoxyribonucleic (DNA) in micro-hematocrit tubes with a fluorescent dye. The QBC test has been proved to be fast and receptive for malaria diagnosis (Salmani Manjunath, Mindolli, & Peerapur, 2011). Although QBC is simple, it requires unique instrumentation and is more costly and inadequate at determining parasites than the conventional light microscopy (Tangpukdee et al., 2009).

Also, conventional diagnosis of sickle cell anaemia is determined clinically by performing High-Performance Liquid Chromatography test (HPLC), the Sickling test by using Sodium metabisulfite and HB electrophoresis (Inusa, Hsu, Kohli, Patel, & Ominu-evbota, 2019; Robert et al., 2002; Tidy, 2015).

These conventional methods can be strenuous resulting in the inability of laboratory technicians to cope with the workload of cross checking-routine slide due to inadequate human resources. Manual microscopic counting of P.

falciparum is also time-consuming and can sometimes be biased. Accurate laboratory diagnosis is essential as inaccurate results can lead to severe consequences, especially for sickle cell patients (Opoku-Ansah et al., 2020; WHO, 2016).

Numerous techniques have been used for the assessment of malaria parasites. Some of these techniques are uses of multispectral imaging technique in identifying wavelength markers for malaria-infected and uninfected red blood cells (Opoku-Ansah, Eghan, Anderson, & Boampong, 2014), identifying malaria parasites using cellphone microscope (Agbana et al., 2018). The use of 3D printed shearing digital holographic microscopy in the diagnosis based on spatiotemporal cell dynamics analysis (Javidi et al., 2018) is a technique developed for the assessment of sickle cell. All these techniques consider the diagnosis of malaria and sickle cell individually. However, there are few to no technique which looks at how sickle cell infected with malaria is identified. Little, however, has been said about how a sickle red blood cells infected with malaria is identified, making the treatment of sickle cell patients infected with malaria risky.

Multispectral imaging microscopy technique (MSIM) has been used in many fields, emphasizing on biological and medical fields (Adueming et al., 2017; Hiraoka, Shimi, & Haraguchi, 2002; Levenson & Mansfield, 2006; Levenson, Lynch, Kobayashi, Backer, & Backer, 2008; Jen, Huang, Chen, Kuo, & Wang, 2014; George et al., 2004; Fountaine, Wincovitch, Geho, Garfield, & Pittaluga, 2006; Rigacci et al., 2000; Bickford, Sun, & Fu, 2008). The multispectral imaging microscope (MSIM) is an optical technique that takes images of microscopic images at two or more wavelengths. It also enables the

extraction of physical and chemical properties information out of the images. MSIM is dependent on the light source used during acquisition. It homogenizes the strength of light imaging microscopy with that of spectroscopy to complete tasks that each cannot perform individually.

The product of an MSIM system is a stack of images of the same object or scene, each at a different spectrally narrow band. MSIM can record light from wavelengths beyond the visible light range, such as infrared (IR).

These measurements allow extraction of additional information that the human eye fails to capture with its receptors for RGB. For accurate reproduction of the original colour through digital imaging systems, the MSIM technology is promising. By using the spectral information, the reproduced colour accuracy is considerably improved as compared to conventional RGB based systems (Hu et al., 2005; Teikari, 2008).

Scope of work

This study aims to culture malaria parasite in sickle RBCs in vitro and classify red blood cells (RBCs) from thin blood smear on thin-film slides of the cultured sample with Giemsa stain as infected RBCs and uninfected RBCs. Secondly, this study focuses on utilizing multispectral imaging techniques to detect and discriminate sickle red blood cell infected with malaria parasites in human blood media with the intent of performing expeditious malaria diagnosis. Discriminating sickle red blood cell infected with malaria parasites is done by imaging the Giemsa stained thin blood smears using a multispectral imaging microscope to capture images in the transmission mode to acquire wavelength

markers for sickle malaria-infected RBCs. An analysis is then done by using Principal Component Analysis (PCA).

Statement of Problem

The effect of malaria on sickle cell anaemia changes the characteristics of the sickle cell. However, sickle cell infected with malaria has not been optically studied; hence, there is a need to develop an objective tool which will aid in discriminating between *Plasmodium*-infected and uninfected sickle red blood cell for early diagnosis.

Research Question

How possible is to discriminate between *Plasmodium*-infected and uninfected sickle red blood cells?

Research Objective

The objective of this work is to study infected sickle red blood cell using multispectral imaging technique. Specifically, the study will look into how to discriminate between infected and uninfected sickle red blood cells.

Significance of Study

This research aims to develop wavelength markers with the help of the Multispectral Light Emitting Diode Imaging system (MSLEDIMS) in discriminating between *Plasmodium*-infected and uninfected sickle red blood cell. The developed marker will aid in the early diagnosis of sickle cell patients infected with malaria.

Organization of Thesis

This thesis consists of five main chapters; chapter one to five. Chapter one gives the background on sickle cell and its diagnosis, malaria and its diagnosis, sickle cell disease infected with malaria as well as a multispectral imaging system. The scope of the work and the organization of the thesis are also included in this chapter. Chapter two reviews the literature on sickle cell and malaria, optical imaging spectroscopy, optical microscopy and multispectral imaging microscopy, and the principle underlying the experimental techniques used in this work.

Chapter three looks at the culturing of malaria parasite in sickle RBCs and the experimental methods for the research work. Chapter four discusses the results, analysis from the images acquired during the experiments. In the fifth chapter, summary and conclusions are drawn and relevant recommendations given to abet further research in this area.

Chapter Summary

The chapter provides an overview of sickle cell anaemia and malaria and their various modes of diagnosis. The background to multispectral imaging technique has also been discussed. The scope of work and organization of the study is included in this chapter.

CHAPTER TWO

LITERATURE REVIEW

Introduction

In this chapter, a discussion will be made on different processes that occur when light interacts with matter, followed by the literature review on spectroscopy with emphasis on multispectral imaging. The latter part gives a review of the data analysis technique and sickle cell disease.

Spectroscopy

Spectroscopy utilizes radiation to acquire information on the structure and properties of matter (Nonell & Viappiani, 2008). Spectroscopy also deals with measurement and analysis of spectra resulting from the interaction of matter with electromagnetic radiation. It involves absorption, emission or dispersion of electromagnetic radiations by atoms and molecule (Meštrović, 2019). Electromagnetic radiation, including visible light, refers to any sort of illuminated energy that is disseminated as waves. The waves properties of frequency (ν), wavelength (λ), and velocity (c) describe electromagnetic radiation (Zumadahl, 2007). All electromagnetic radiations travel in a vacuum at a constant velocity: c = 3.00 x 10^8 m/s, the speed of light. Frequency and wavelength are inversely related, and their product equals velocity:

$$\nu = \frac{c}{\lambda} \quad (1)$$

The energy (E) of electromagnetic radiation is directly proportional to its frequency:

$$E = h\nu \tag{2}$$

where; h is the Planck constant (h=6.626x 10^{-34}J. s)

The full range of electromagnetic radiation wavelengths is known as the electromagnetic spectrum. There are several bands of the electromagnetic spectrum which are separated according to their wavelengths. The wavelengths between 380 nm and 730 nm represent the visible band (Nelson, 2014b) as presented in figure one.

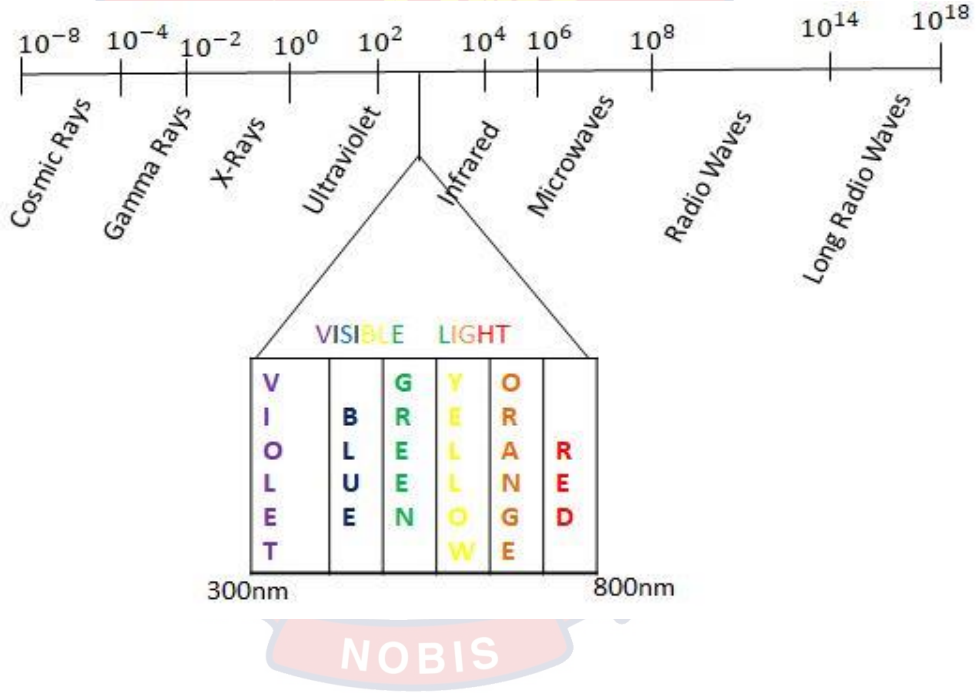

Figure 1: The electromagnetic spectrum showing the visible light (Nelson, 2014)

The visible portion of the electromagnetic spectrum can be discerned visually; human eyes perceive these wavelengths as various colours. The human eye interprets a single or limited presence of wavelength as a specific colour. In the presence of a single wavelength, it is referred to as monochromatic light.

When all the wavelengths of visible light are present, it is classified as white light. However, when there are no wavelengths present in the visible range, it is interpreted as dark. Light cannot travel faster than its velocity, C, in a vacuum which is 2.99793 x 10^{10}cm/sec, but if it travels through a substance, its velocity will decrease (Cones, 1996). Hence,

$$C = \nu\lambda \tag{3}$$

The frequency of vibration, ν, is always constant when the light passes through any material. If the velocity C is reduced during its passage through an object, the wavelength λ must also be reduced. Refractive index, n, of a material is defined as the ratio of the velocity of light in a material C_m through which it passes, to the velocity of light in a vacuum, C.

$$n = \frac{C}{C_m} \tag{4}$$

The refractive index of a material is always higher than 1.0, indicating that C_m is always less than C. C_m depends on the density of the material and hence C_m is inversely proportional to density. Therefore, the higher the density of a material, the higher its refractive index. The refractive index of any material is reliant on the wavelength of light since the atoms that make up the substance interact with different wavelengths at different degrees. The refractive index usually varies linearly with wavelength (Nelson, 2014).

Photons of light can be obliterated, redirected or converted into lower energy photons when they pass through a substance. Thus, light can be transmitted, scattered and refracted. Figure 2 shows the interaction of light with a matter.

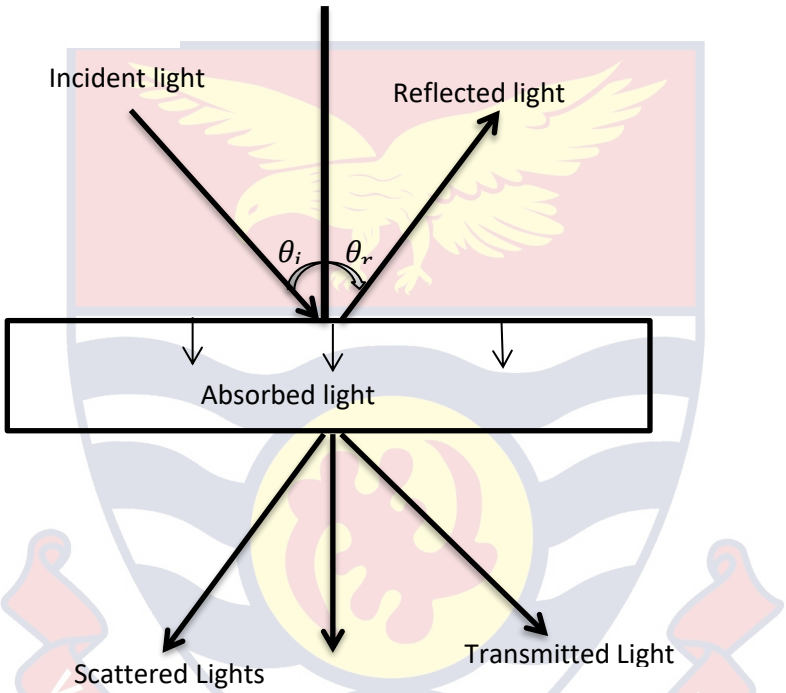

Figure 2: The interaction of light with matter, showing Reflection, Absorption, Transmission and Scattering phenomenon (Svanberg, 2003).

A light that moves in a straight line through a homogeneous medium as a ray continues until it interacts with some material or object (Gupta, Ghosh, & Banerjee, 2015). Several conditions occur when light interacts with the boundary between two materials. Some of the light gets reflected into the material it originated from, whiles part gets transmitted into the second medium.

The transmitted light may or may not be absorbed. Refraction occurs when the propagating direction of transmitted light changes as it crosses the boundary between two materials. Whenever light propagates through a substance without considerable scattering, the material is said to be transparent. On the other hand, when there is a significant amount of scattering the material is said to translucent. Materials which let no light to penetrate through them are said to be opaque (Zhang et al., 2012).

When a ray or wave of light strikes the interface between two different media, all of or part of the wavefront returns into the medium from which it originated from, this phenomenon is known as a reflection (Albregtsen, 2008). The measure of light reflected by an item, and the way it is reflected, is profoundly reliant on the nature of the surface. Reflection can be either specular or diffuse. A surface is determined as a smooth surface when its surface variation is lesser than the wavelength of the light incident on it (Gordon, Beichner & Serway, 2000). When light strikes a smooth surface, specular reflection causes the angle of the incident to be equal to the angle of reflection (Pūtaiao, 2012).

$$\theta_i = \theta_r \tag{5}$$

where

θ_i = the angle of incident, θ_r = the angle of reflection

Though the angle of reflection is the same as the angle of incident in diffuse reflection, diffuse reflection occurs when light strikes on a rough surface causing it to reflect irregularly in different directions.

Scattering occurs when light interacts with small particles such as atoms or molecules. Scattered light spreads in many directions and tends to be scattered over and over again until it is finally absorbed. Scattering is the basis to why the sky is blue and why the sky looks reddish (Gupta et al., 2015). Reflection, refraction and diffraction are all forms of scattering. Regardless, whether light is not of a resonance frequency, weak scattering impacts are still acquired, resulting in Rayleigh and Raman scattering (Bohren & Huffman, 1983). Rayleigh scattering occurs when the elastic scattering of light from atomic and molecular particles diameter is one-tenth less than the wavelength of the incident light (Xu, 2002).

According to Stark effect, an electric dipole moment P is induced in a polarized particle if the particle is subject to an electric field of resultant amplitude (E), initial amplitude (E_o), frequency (ν) and time (t) as shown in equation 6, the polarization can differ for frequency.

$$E = E_\circ \sin\left(2\pi\nu t\right) \tag{6}$$

The total radiated intensity of Rayleigh scattered light I is of the form

$$I = \frac{16\pi^4 c\alpha^2 E_\circ^2}{3\lambda^4} \tag{7}$$

where α is the polarizability tensor, c is the speed of light and λ is the wavelength of the light source. Equation 7 shows that the intensity of Rayleigh scattered light decreases when the fourth power of wavelength of light source increases (Gauglitz, 2003; Svanberg, 2003).

Mie scattering, which is elastic, occurs when light incident on particles of size transcending the light wavelength. Equation 8 is used to calculate the probability of Mie scattering.

$$\sigma_{Mie} = f(x, m_{rel}) \tag{8}$$

Where

$$x = \frac{2\pi r}{\lambda}, m_{rel} = \frac{m_1}{m_2} \tag{9}$$

$$m_1 = n - ik, \quad \text{For air} \quad m_2 \approx 1$$

λ is the wavelength, r is the particle radius, m_1 the complex of the index of refraction and, m_2 is a corresponding quantity for the surrounding medium.

σ_{Mie} changes quickly as an element of the parameter *x* due to interference impacts identified with surface waves on particles. For regular molecule conveyances in the particles, the motions are spread out while the scattering intensity changes gradually with the wavelength. The intensity increases with an estimated, λ^{-2} dependency on shorter wavelengths. When looking at atmospheric molecules, Mie scattering is of great importance to Rayleigh scattering.

Mie scattering, which can also be used to detect particles in ambient air and water, determines atmospheric visibility (Albregtsen, 2008).

It does not matter whether light is being weakened by absorption or scattering. In the two cases, the transmitted intensity will diminish exponentially with the thickness *x* of the material the light is going through. If the attenuation is

due to absorption, the transmitted intensity I is usually written as in equation (10) (Lars, 2019).

$$I = I_{\circ} \cdot 10^{-\alpha x} \tag{10}$$

whereas if the attenuation is due to scattering the intensity is written as

$$I = I_{\circ} \cdot e^{-\tau x} \tag{11}$$

where, I_O is the incident intensity before attenuation, α is the absorption coefficient, τ is turbidity, e and 10 are the exponential decays.

Optical Imaging Spectroscopy

Imaging generally refers to capturing, storing and displaying of images. Optical imaging is a technique for non-invasively examining the internal structure of bodies (Hecht, 2002). To acquire detailed images of organs and tissues as well as cells and molecules, optical imaging utilizes light from the optical region and the special properties of photons. The strategy for spectroscopy, using an appropriate light source and other devices for radiation examination, has its standard field of utilization in the determination of the general energy-level structure in the energy range corresponding to UV, visible and IR light (Dolloff & El-Deiry, 2009). The optical spectroscopy wavelength range extends from 200 nm (UV) to 500 nm (Far Infrared (FIR)). It is challenging to construct a single spectral instrument capable of fully covering the area and providing information about the various processes of light absorption, emission and scattering (Gauglitz, 2003). Many optical spectroscopic techniques have been developed to investigate

material properties based on the interactions of electromagnetic radiation with matter.

In general, imaging spectroscopy obtains the spectrum of the energy of each spatial resolution element of an image. Such spectra are used to extract knowledge based on the signature of the spectrum interaction of matter and energy. Examples include spatial classification based on spectral signatures, use of substance recognition spectral libraries, a study of mixture composition, plume detection, etc. (Gat, 2000). Simultaneous imaging in multiple spectral bands across the spectrum allows us to "see" details exceeding the capabilities of the human eye (Coffey, 2012). Imaging done at spectral bands between 2 to 100 µm results in multispectral imaging and hyperspectral imaging having more than 100 spectral bands. There are various applications of multispectral and hyperspectral imaging systems (Charles, Mark, & Migue, 1996; Fischer, Kakoulli, Fischer, & Kakoulli, 2013; Freeman et al., 1997; GIS Geography, 2015; Hong & Xiang, 2020; Jianwei, Kuanglin, Moon, Renfu, & Thomas, 2013). These technologies have applications in fields that range from environmental monitoring, military surveillance, and many others.

Optical Microscopy

In the past century, optical microscopy has seen tremendous development in its application for study on a wide range of disciplines on the micron and submicron level. The fast expansion of novel microscopic instruments has increased and simplified its uses in various laboratories (Muller, 2019). The diverse approaches in digital imaging and analysis have made it possible for

microscopist to get hold of quantitative measurements fast and efficiently on specimens ranging from photosensitive compounds to real-time fluorescence microscopy of living cells in their habitat (Davidson & Abramowitz, 2002).

Presently, the most efficient and reliable diagnostic technique is optical microscopy. It is highly sensitive and specific in the sense that samples are visualized and identified by their features. The influences of optical microscopy are diverse: it is feasible to discriminate between species, quantify parasitaemia and monitor asexual stages of parasites. Optical microscope resolution determines the shortest distance between two points on a sample that can be distinguished at different points by the observer or camera device (Vander Voort, 2005). In optical microscopy, resolution can be said to be somewhat subjective since an image can appear fuzzy at high magnification but still be resolved to the full capacity of the objective. Its numerical aperture determines the resolving power of an objective. Still, the overall resolution of the whole microscope optical train is also reliant on the numerical aperture of the substage condenser. The resolution of the total system is improved with a higher numerical aperture (Davidson, 2020). The sub-stage condenser must be coordinated to the objective regarding the numerical aperture and regulation of the aperture iris diaphragm for detailed light cone structure and specimen illumination. The light wavelength range used to image a sample is also a deciding factor in the resolution level given by the microscope. In comparison to longer wavelengths, shorter wavelengths are more capable in resolving details to a higher degree. To determine the relationship between numerical aperture, wavelength, and resolution, several relations such as equations 12, 13 and 14 have been derived. (Spread, 2019)

$$r = \frac{\lambda}{2NA} \tag{12}$$

$$r = \frac{0.61\lambda}{NA} \tag{13}$$

$$r = \frac{1.22\lambda}{(NA(obj) + NA(cond))} \tag{14}$$

where, r is the resolution, NA is the numerical aperture, NA (obj) is the objective numerical aperture and NA (cond) is the condenser numerical aperture

Multispectral Imaging Microscope

Multispectral imaging helps obtain images corresponding to some spectral bands. These spectral regions cover the Ultra-Violet (UV), visible and near infra-red region of the electromagnetic spectrum. Even though human eyes can easily distinguish millions of colour combination, they cannot see all-optical and spectral ranges of colours. The reason is that the human eye separates visible light, no matter how complex it is into three components which are red, blue and green (RGB) which are the primary colours of light (Henderson, 2015).

The multispectral imaging microscope (MSIM) consists of a multispectral illuminator with a selectable spectral composition. It is obtained when optical imaging spectroscopy is done at several spatial locations at the microscopic level, with transmittance and at several wavelengths. Most optical analyses aim to extract all information from the sample of which there is a limit to it. Spectroscopy, however, aims to determine and explain how photons are emitted. This potential has aided the rise in multispectral imaging microscopy. A charge-

coupled device (CCD) camera coupled with coloured filters of distinct spectral bands, ranging from three to hundreds of elements, is used for multispectral imaging microscopy (Nieves et al., 2005).

The multispectral imaging microscopy systems are not crafted to analyze a large portion of the electromagnetic (EM) spectrum; this is due to the possibility of missing important information contained in the non-sampled bands. In-depth analysis of the sample can be done over a small portion of the spectrum (Opoku-Ansah, 2014). Due to the availability of endless information provided by the MSIM, it would be very costly and inefficient to collect all data throughout the electromagnetic spectrum. The imaging device is capable of simultaneously collecting spectral data from several regions in space discredited, leading to both the collection of spatial and spectral data from many points in a three-dimensional image. The acquisition process and components involved in a multi-spectral imaging system are described schematically in figure 3.

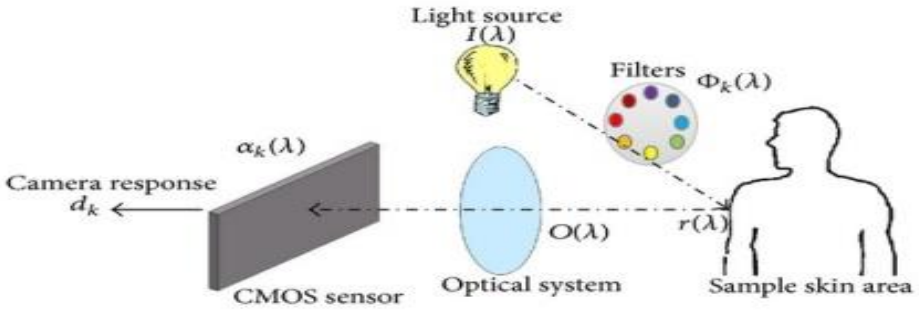

Figure 3: Outline of a spectral model showing the process of acquisition in a multispectral system (Jalil, 2008)

In figure 3, I(λ) is the spectral radiance of the illuminant, r(λ) is the spectral reflectance of the surface, O(λ) is the spectral transmittance of the optical system, Φ_k (λ) is the spectral transmittance related to the k^{th} filter and a(λ) is the spectral sensitivity of the camera. The camera output d_k, related to the channel k for a single pixel of the image, is given by equation 15,

$$d_k = \int_{\lambda\min}^{\lambda\max} I(\lambda) r(\lambda) O(\lambda) a(\lambda) d\lambda \tag{15}$$

Supposing a linear optoelectronic transfer function, $I(\lambda)$, $a(\lambda), o(\lambda)$ and $\Phi_k(\lambda)$ can be substituted by the spectral sensitivity $S_k(\lambda)$ of the k^{th} channel. Then, equation (15) becomes:

$$d_k = \int_{\lambda\min}^{\lambda\max} r(\lambda) S_k d\lambda \tag{16}$$

Sampling the spectra to N wavelengths, equation (16) can be written in matrix notations as in equation (17) as

$$d_k = r(\lambda)^T S_k(\lambda) \tag{17}$$

$S_k(\lambda) = [s_k(\lambda_1) s_k(\lambda_2) ..... s_k(\lambda_N)]^T$ is the vector that comprises the acquisition system's spectral sensitivity associated with the k^{th} channel.

$r(\lambda) = \left[r(\lambda_1) r(\lambda_2) .... r(\lambda_k) \right]^T$ is the vector of the sampled spectral reflectance of the scene.

$[]^T$ is the transpose operator.

Equation 17 helps to describe the system's spectral response, including the camera and the illuminant, by finding the $\mathbf{S}_k(\lambda)$ operator. The spectral reflectance curve for each pixel of the imaged scene is reconstructed from the multispectral image using the operator $\mathbf{S}_k(\lambda)$ (Mansouri et al., 2005).

Applied Multivariate Analysis Techniques

The multivariate analysis comprises of techniques which are used for data extraction and analysis. Examples of applied multivariate analysis techniques are principal component analysis (PCA), multiple correspondence analysis (MCA), multidimensional scaling (MDS), multiple linear regression analysis (MLR), correspondence analysis (CA), partial least square regression (PLSR), principal component regression (PCR) and ridge regression (RR).

Principal Component Analysis (PCA) is a way to define knowledge trends in a way that draws attention to their similarities and differences. Since data trends can be challenging to determine in high dimensional data, PCA is a valuable tool for data analytics (Smith, 2002). PCA requires a linear transformation of the data such that the projection of the data has the most significant variance along the first axis, defined as the first principal component, second highest variance along with the second principal component, and many more in the new coordinate frame**.** The number of principal components used depends on the accuracy level needed to recreate the original data set (Alkrimi, Tome, & George, 2019). The analysis is aimed at modelling the structure of the variance-covariance of a data matrix from which the eigenvalues corresponding to

the main components are derived. A linear combination of the original variables is of each principal component (Ferrer-Galindo et al., 2018).

Considering a multidimensional data set, X of *n* observations occurring in *m* dimensions or variables, the method used in measuring the data, is shown as

$$X = \begin{bmatrix} x_{11} & x_{12} & \cdots & x_{1m} \\ x_{21} & x_{22} & \cdots & x_{2m} \\ \vdots & \vdots & \ddots & \vdots \\ x_{n1} & x_{n2} & \cdots & x_{nm} \end{bmatrix} \quad (18)$$

Obtaining the mean vector from X:

$$\bar{x} = (\overline{x_1}, \ldots\ldots\ldots, \overline{x_j}, \ldots\ldots\ldots, \overline{x_m}) \quad (19)$$

Where:

$$\overline{x_m} = \frac{1}{n}\sum_{i=1}^{n} x_{im} \quad (20)$$

is the mean of each variable in the multidimensional data set.

$$\sigma_k = \sqrt{\frac{\sum_i^n (x_{im} - \overline{x_m})^2}{n}} \quad (21)$$

Each variable is subtracted from its mean value, and the result is divided by the standard deviation (σ_k), the influence of each variable is normalized to get a new matrix, Y

$$y_{im} = \frac{x_{im} - \bar{x}_m}{\sigma_i} \tag{22}$$

$$Y = \begin{bmatrix} y_{11} & y_{12} & \cdots & y_{1m} \\ y_{21} & y_{22} & \cdots & y_{2m} \\ \vdots & \vdots & \ddots & \vdots \\ y_{n1} & y_{n2} & \cdots & y_{nm} \end{bmatrix} \tag{23}$$

proceeding to obtain the covariance matrix **S**, given by:

$$S = \frac{1}{n} Y^T Y \tag{24}$$

where Y^T is the transpose of Y an $1/n$ is a constant for normalization with n still denoting the number of observations in X. This covariance matrix provides essential information on the spread of the variable values in X. The S is a square symmetric matrix, v x v, with the v diagonal elements being the variances of X of particular measurement types. Proceeding to obtain the values and eigenvectors, using the equation

$$\left| S - \lambda I \right| = 0 \tag{25}$$

Once eigenvectors are found from the covariance matrix, a feature vector (V) is then formed from the eigenvectors in columns. The function vector (V) generated using the covariance matrix's eigenvectors is used to reorient the data from the original axes to those described by the principal components. This is be done by

$$T = V^T \times Y^T \tag{26}$$

where T is the new data set for PCA.

The variability percentages were obtained by:

$$VarT_i = \frac{\lambda_i}{n} \times 100 \tag{27}$$

Characteristics of Sickle Cell

Sickle cell anaemia is a blood condition in which, when viewed under a traditional microscope, red blood cells (RBC) show an irregular sickle shape as shown in figure 5. In the DNA sequence of the gene encoding the haemoglobin beta chain (beta-globin gene), the cause of sickle cell anaemia was directly attributed to a single base substitution (Ciencia & A, 2011). There is a need to have two altered haemoglobin genes for a patient to develop Sickle Cell Disease (SCD), one from each parent. If a patient inherits only one of these genes, the patient will have sickle cell trait, which is very much milder than the sickle cell disease. Figure 4 shows a graphical representation of possible outcomes if two parents with sickle cell trait have a child. There are several varieties of sickle cell disease. Some are Sickle Cell Anemia (SS), Sickle Hemoglobin-C Disease (SC), Sickle Beta-Plus Thalassemia and Sickle Beta-Zero Thalassemia (Kanchanawong, 2017).

i. **Sickle Cell Anemia (SS)**: This occurs when a child inherits one substitution beta-globin genes (the sickle cell gene) from each parent.

ii. **Sickle Hemoglobin- C Disease (SC)**: People with sickle Hemoglobin-C Disease (SC) have slightly different circumstances. Their beta-globin genes

produce both haemoglobin C and haemoglobin S. Sickle Hemoglobin-C disease may cause similar symptoms as sickle cell anaemia.

iii. **Sickle Beta-Plus Thalassemia**: In both beta-globin genes, individuals with Sickle Beta Thalassemia (SB) disorder also produce substitutions. Depending on the amount of normal beta-globin produced, the severity of the disease varies. The symptoms are almost similar to sickle cell anaemia when no beta globin is made, with extreme cases requiring chronic blood transfusions.

iv. **Sickle Hemoglobin-D Disease**: Research has shown that haemoglobin D, which also interacts with the sickle haemoglobin gene, is a distinct replacement for the beta-globin gene. Those with sickle haemoglobin-D (SD) disorder have relatively severe anaemia and occasional episodes of pain

v. **Sickle Hemoglobin-O Disease**: Hemoglobin O also interacts with haemoglobin in the sickle. Individuals with sickle haemoglobin-O (SO) disorder experience symptoms that are too similar to sickle cell anaemia (Williams, 2017).

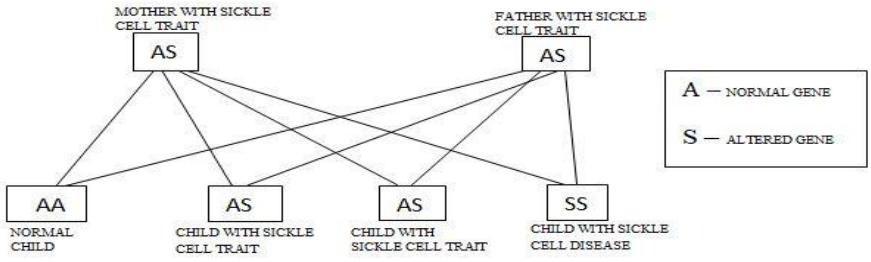

Figure 4: A graphical representation of possible outcomes if two parents with sickle cell trait have a child (Wilkie & Werley, 2013).

Figure 5: An image of normal red blood cell and a sickle-shaped red blood cell (https://www.mayoclinic.org/diseases-conditions/sickle-cell-anemia)

Early in life, SCD is characterized by extreme chronic hemolytic anaemia caused by sickle and vaso-occlusion haemoglobin, bacterial infection and organ infarction, including brain infarction. Acute chest syndrome (ACS) is one of the complications of sickle cell disease, characterized by the onset of chest symptoms, new pulmonary infiltration on the chest radiograph, and, in some cases, fever, cough, dyspnea, and chest pain (Ogedegbe, 2018).

Medical researchers working in Africa proposed in 1949 that sickle cell gene carriers were immune to falciparum malaria, establishing a connection between molecules and selective pressure. The inheritance of this variant haemoglobin gene (S) has been suggested to confer resistance to falciparum malaria in the heterozygous state, which is frequently lethal in the early years of existence (Friedman, 1997). Ana Ferreira, a post-doctoral researcher in Miguel Soares' laboratory, confirmed that the sickle haemoglobin does not succumb to cerebral malaria. This protective effect is caused by Heme Oxygenase-1 (HO-1), an enzyme whose expression is strongly triggered by sickle haemoglobin (Ciencia & A, 2011).

With this discovery made, identification of sickle cell patient with malaria optically should have been easy, but this is not so. Sickle cell patients go through the same process as ordinary patients in identifying malaria parasite in their blood

via microscope by quantifying malaria parasites against the RBCs. This is done by counting the parasitized RBCs among 500-1,000 RBCs on the thin smear slide, and the result is expressed as % parasitaemia as shown in equation 28.

$$\%\, parasitaemia = \frac{parasitised\ RBC\ counted}{total\ \ RBCs\ counted} \times 100 \tag{28}$$

Traditional counting, which is based on the examination of Giemsa stained thin blood smears under a microscope, is inappropriate and inaccurate in many ways. The ability of a technician to detect malaria depends on the number of microscope fields examined (Ross et al., 2006). Parasite or non-parasite identification, even for humans, is not an easy task without special training (Tek et al., 2009).

Chapter Summary

This chapter reviewed the literature on spectroscopy with emphasis on multispectral imaging. In addition, the chapter provides a review on multivariate data analysis techniques and sickle cell disease.

CHAPTER THREE

RESEARCH METHODS

Introduction

This chapter describes the experimental methods and procedure for blood sample collection and data acquisition. The first part of the chapter looks at the process of collection and preparation of blood samples. The second part of the chapter presents the protocol for culturing the plasmodium parasite into the blood samples. The final part of this chapter focuses on the description of the Multispectral Light Emitting Diode Imaging Microscope (MSLEDIM) system and procedure for the acquisition of multispectral images from the Multispectral Light Emitting Diode Imaging Microscope (MSLEDIM).

Blood Sample Collection

In the laboratory at the Cape Coast Teaching Hospital (CCTH), an amount of 2 ml blood samples were collected from people (volunteers) by a laboratory technician. Electrophoresis was then used to pass an electrical current through the haemoglobin of the blood samples to determine the different haemoglobin groups. The results obtained were compared to healthy samples to select those that were sickling positive and those that were not. An amount of 5 ml blood was collected from two volunteers who tested sickling positive and one non-sickling patient. The sample was stored in a yellow-top vacutainer (This tube contains acid citrate dextrose (ACD)), which is used for the collection of whole blood for special tests). The vacutainer was moderately inverted nine times to ensure the proper anticoagulation of the specimen. The process was to ensure adequate mixing.

It was then placed in a blood transport container for them to be transported to the department of parasitology at the Noguchi Memorial Institute for Medical Research (NMIMR). At the NMIMR, the samples were then transferred from the transport container and stored in a refrigerator at a temperature of 4 ± 2 ℃. Each sickle cell blood sample was then taken out to be washed for plasmodium culture.

Protocol for Culturing Malaria Parasites

Washing of Human O+ Donor RBCs for Plasmodium Cultures

The stored refrigerated samples were washed (removing most of the white blood cells, plasma and platelets) before they were used in plasmodium culturing. Before washing of the blood samples, a Complete Parasite Medium (CPM) was made by pipetting 2.5 ml of Gentamicin into a flas000000k, then adding 50 µl of 200 mM 1-glutamine and lastly 50 ml of Albumax II. By moderately inverting the flask eight times, the reagents are mixed and filtered using a 0.20 µm sterile filter and stored at a temperature of 4 ± 2 ℃.

The filtered red blood cells samples were stored in a refrigerator at 4 ± 2 ℃ up to forty-eight hours before processing. The stored blood samples in the vacutainer were placed in a centrifuge and spun at 2000 rate per minute (rpm) for seven minutes. The spun blood samples were transferred into a Biological Safety Cabinet (BSC). With a serological pipette, which was changed for each sample, the serum and buffy coat found on top of the packed red blood cells after spinning (this layer contains white blood cells) were carefully aspirated. All tubes and flasks are sprayed with 70 % alcohol to sanitize them before they are placed in the BSC. The packed red blood cells that were left after aspiration was transferred

into a sterile 15 ml falcon tubes using a 10 ml pipette, re-suspended in parasite wash medium (PWM) in a ratio of 1-part blood: 3 parts PWM. The mixture was mixed thoroughly by pipetting up and down and centrifuged at 2000 rpm for ten mins. The process of suspending in PWM and centrifuging was repeated after the supernatant was aspirated in the BSC. After the sample has been centrifuged three times, the supernatant was aspirated in the BSC, and the packed red blood cells were finally re-suspended in PWM at a ratio of 1-part blood: 3 parts PWM and was stored in the refrigerator for plasmodium culturing.

Thawing of parasites

Malaria parasites used for culturing were kept in a vial and preserved by keeping it frozen with liquid nitrogen at -180 ℃. The vial containing frozen parasites was removed from the liquid nitrogen tank and placed gently in a water bath set at 37 ℃ (with the screw cap top of the vial above the water surface) for one to two mins. This vial was allowed to slightly thaw while gently tapping the bottom of the vial intermittently. The slightly thawed parasite in the vial was then spun down in a centrifuge at 1500 rpm for ten (10) mins. It was ensured that the vial was not spun above the set speed to prevent lysing of the parasites. After spinning the vial, its exterior was carefully wiped and sanitized with 70 % alcohol. This sample was placed in the BSC, where the parasite was transferred into a T25 flask. An amount of 0.5 ml fresh RBC's was added to the parasites in the T25 flask to ensure the smooth growth of the parasites. Gas (compressed mixed gas, i.e. 92.5 % nitrogen, 5.5 % carbon dioxide and 2 % oxygen) was

supplied into the T25 flask containing the parasites for two to three mins then stored in an incubator at 37 ℃, 110 % carbon dioxide for in vitro culturing.

Synchronization of parasite

Synchronization of plasmodium parasites helps in bringing cells in the culture at different stages of the cell cycle to the same phase. Parasite synchronization involves two processes; these are Sorbitol synchronization and percoll synchronization. For parasite synchronization, sorbitol synchronization is done before percoll synchronization.

Sorbitol synchronization

When the ring population of the thawed plasmodium parasites stored in the incubator reaches 5 %, sorbitol synchronization is done. During sorbitol synchronization, an amount of 5 % sorbitol solution was warmed to a temperature of 37 ℃ in a water bath. In the BSC, the culture was transferred into a 15 ml tube and spun in the centrifuge at 2000 rpm at 37 ℃ for five mins. The spun 15 ml tube was transferred into the BSC, and the medium above the pellet (two layers were observed after spinning, the pellet and the solution above it) was discarded. The remaining pellet after the medium was discarded was re-suspended with sorbitol solution to its original volume and mixed thoroughly by moderately inverting the tube ten times. Mixed sample was placed into the incubator for ten mins and was spun for five mins at 2000 rpm at 37 ℃. The spun sample was transferred into the BSC, the supernatant discarded, and the pellet washed three times with 10 ml of CPM (which the supernatant was discarded after every spin)

at 2000 rpm for five min at 37 ℃. After the last spin-off, the pellet and the medium above is discarded, the remaining pellet was transferred into a new flask, and an amount of 100 µl of fresh RBCs was added to it, gased for three mins and placed into the incubator for percoll synchronization.

Percoll Synchronization

In percoll synchronization, three different percoll reagents (90 % percoll, 65 % percoll and 35 % percoll) were prepared and used for the synchronization. Firstly, 90 % of percoll-PBS was prepared by mixing 2 ml of 10X phosphate Buffer saline (PBS) with 18 ml of 100 % percoll. From the 90 % percoll-PBS prepared, 6.5 ml was pipetted into a 15 ml flask and mixed with 2.5 ml of PWM to obtain 65 % percoll. Also, 35 % percoll was prepared by mixing 3.5 ml of 90 % percoll-PBS with 5.5 ml of PWM.

In the BSC, the culture was transferred into a 15 ml flask and was centrifuged at 2000 rpm for 5 mins at 37 ℃; the supernatant was discarded, and the pellet was re-suspended with 2.5 ml CPM. Using a Pasteur pipette, 3 ml of 65 % percoll was pipetted into a 15 ml flask; 3 ml of 35 % percoll was gently added on top by tilting the tube to 60 % and allowing the percoll solution to run along the sides of the tube. On top of the freshly prepared percoll gradient, 2.5 ml cell suspension was slowly layered (care was taken not to mix it with the percoll gradients). Without a break, the suspension was centrifuged in a swing-out rotor at 2500 rpm for fifteen mins at room temperature. Five distinct layers were observed after the suspension spinning; these were from top to bottom, the cell suspension layer, 35 % percoll layer, lower interface (parasitized RBCs), 65 %

percoll layer and pellet (RBCs and early-stage parasites). Four of the distinct layers observed were discarded, leaving the lower interface of the cell suspension, which was transferred into a new tube and was spun down at 2000 rpm for five min. The supernatant was discarded, and the remaining pellet was washed twice with 10 ml PWM and spun at 2000 rpm for five min. After washing with PWM, the remaining pellet was washed twice again using 5 ml CPM and spun at 2000 rpm for five min after which the supernatant was discarded leaving the remaining pellet (20 µl) which was used for the culturing.

Plasmodium Culturing

The washed blood samples SS, AS and AA were removed from the refrigerator and thawed in a water bath at 37 ℃ for five mins. Amount of 360 µl blood was taken from each sample and 8640 µl CPM was added to each sample amounting to 9000 µl which was used for the culturing. During the culturing, nine culturing wells were used; each sample was divided into three (3) parts, for which two were used for parasite-infection and one uninfected for control. For the plasmodium culture, 20 µl of the pellet was recovered after the percoll-PBS synchronization and using 4 % haematocrit, as stated in appendix II, a total amount of 500 µl of plasmodium parasite was used for culturing. With six wells being infected, an amount of 83 µl culture was used for each infected wells. In the BSC, using a pipette, the samples and culture solutions were placed into the various culturing wells, as shown in Table 1. The pipette was changed each time a different sample is drawn. The culturing plates were placed in a modular incubator chamber which was tightly sealed and gased for three mins.

After gassing, the modular incubator chamber that contains the cultures was placed in the rudimentary incubator. For 6 days, the incubated samples were monitored daily by changing the CPM, gassing for 3 minutes and putting the samples back into the rudimentary incubator every day.

Table 1: Distribution of plasmodium parasites into the various blood samples for culturing

SAMPLES	IRBC-DAY 1	IRBC-DAY 6	UNINFECTED
AA	3000 µl+83 µl	3000 µl+83 µl	3000 µl
AS	3000 µl+83 µl	3000 µl+83 µl	3000 µl
SS	3000 µl+83 µl	3000 µl+83 µl	3000 µl

A Giemsa stained slide smear was also made daily. The stained slides were then placed in a plastic microscope slide box and transferred to the Laser and Fibre Optic Center (LAFOC) at the University of Cape Coast to calculate the parasitemia growth. Multispectral Light Emitting Diode Imaging Microscope System (MSLEDIMS) was used to take images for further analysis of the various samples.

Multispectral Light Emitting Diode Imaging Microscope System *(*MSLEDIMS*)*

At LAFOC, a Multispectral Light Emitting Diode Imaging Microscope System (MSLEDIMS) was used to take the multispectral images of the Giemsa stained slide smears.

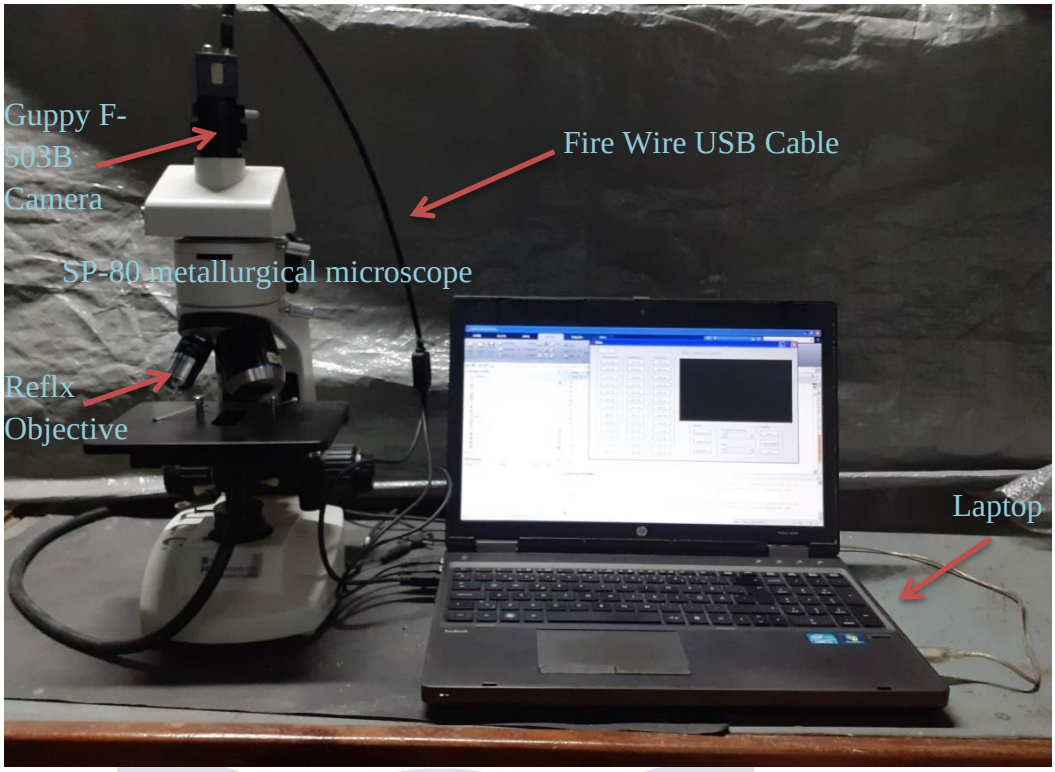

Figure 6**:** Multispectral Light Emitting Diode Imaging Microscope System.

The multispectral LEDs imaging microscope (MSLEDIM) comprises of SP-80 metallurgical microscope, mechanical, optical and optoelectronic components. The mechanical components have LED holders and brass tube. Three separate LED holders were used to hold the LED chips of single, double and triple illumination in reflection, transmission and scattering modes. The LED holders are designed to accommodate and provide electrical interconnection and thermal solution for the LEDs. The holders consist of a heat sink, locking ring, and contact carrier assembly. The holders are designed in such a way that the optical axes of the LEDs strike one common point. For each illumination mode which is a reflection, scattering and transmission, there is an almost identical LED

holder. The only difference between them is the shapes of the edges since they are attached to different parts of the microscope.

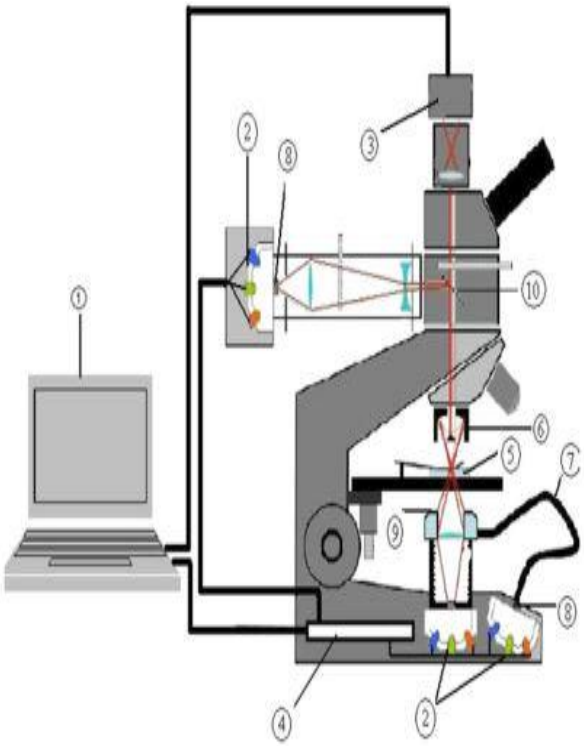

1: Computer
2: LED set
3: Camera Support
4: Data acquisition device
5: Sample stage
6: Objective
7: Optical Fiber
8: Diffuser
9: Coarse and fine adjustments
10: Beam splitter

Figure 7: A schematic diagram of the Multispectral Light Emitting Diode Imaging Microscope

The brass tube is made from brass which has been chemically treated to remove its reflective surface. It fits together with the LED holder, microscope base, and a fibre ring (FR) (Edmund Optics©, 2000). The brass tube serves to adjust the height between the diffuser and the lens and also changes the angle at which light falls on the sample in the dark field (DF) mode. The brass tube has a top-hat which is made from black Delrin to absorb any light that strikes the surface.

The fibre ring, Reflx™ objective, polka-dot beam splitter, optical diffuser and LEDs are the optical component used in the MSLEDIM. The fibre ring consists of many fibres bundled together and guided from a glass-polished end-face into anodized, aluminium housing where it emits diffuse light in 360 ° around the central axis. It has numerous fibres which emit shadow-free light and contribute to the illumination by creating free light. The fibre ring is also used to focus light in between the sample and the objective. Magnification is greater than 1 when the fiber ring is at a long distance from the sample and vice versa.

The Reflx™ objective aids in acquiring quality images over a wide spectral range. It has a magnification of x10 with a Numerical Aperture of 0.25, and it is based on reflective optics. Figure 8 shows an image of an x10 objective.

Figure 8: Image of a Reflx objective

The polka-dot beam splitter is used to illuminate a sample from the same direction the transmitted light is detected and can be optimized to transmit light in a relatively narrow spectral region.

The optical diffuser used to assist the illumination of the incoming light is found at the common point of the optical axes of the LEDs in the holders.

Nine LEDs which emit a total of thirteen different wavelengths, ranging from Ultraviolet (UV) to near-infrared (NIR), are used as illuminating sources in reflection, transmission and scattering modes. The wavelengths are 375 nm, 400 nm, 435 nm, 470 nm, 525 nm 590 nm and 625 nm. The rest are 660 nm, 700 nm, 750 nm, 810 nm, 850 nm and 940 nm. One of the LEDs emits three wavelengths 470 nm, 525 nm and 810 nm. Two others are emitting two wavelengths each that is 375 nm, 625 nm and 400 nm, 850 nm respectively. The remaining LEDs emit a wavelength each. These are 435 nm, 590 nm, 660 nm, 700 nm, 750 nm and 940 nm.

The optoelectronic components comprise of an imager, which is monochromatic with a resolution of 2592 X 1944 pixels with a charge-coupled detector (CCD), is used in capturing images of samples. The data acquisition device (DAQ) (which is used to bridge a computer); the LEDs switch controlling data through a computer algorithm and a multiplexer which controls the connection of the path from the current driver output down to the ground.

Multispectral Image Acquisition

Using a multimeter, the power supply to the microscope was ensured to be nine volts before it was plugged into a power source of the electronic circuit

board. The universal serial bus (USB) from the imager and the data acquisition plate were plugged into their respective port on the computer. The power supply and the laptop were switched on, and the MATLAB program was launched. In the MATLAB program, the start bottom was turned on, and the exposure time was set to ten seconds whiles gain was set to zero.

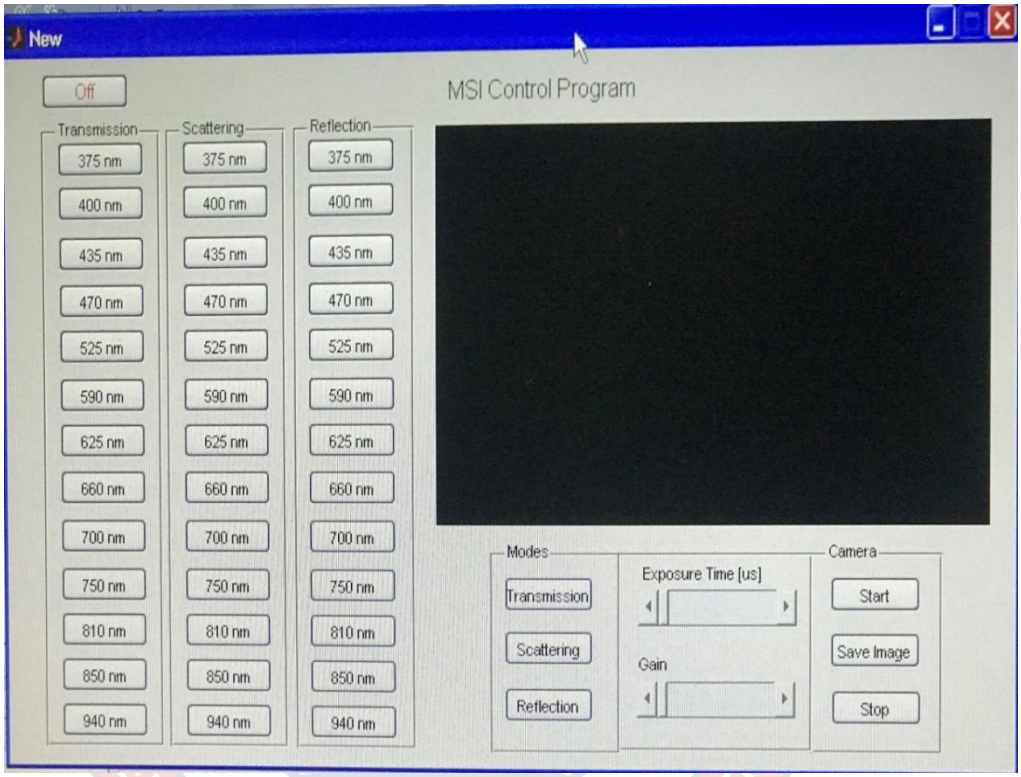

Figure 9: MATLAB Graphical User Interface (GUI) for controlling modes and wavelengths from Camera

Under the modes icon, each mode was selected individually, and images of the sample are taken respectively. Lights from LEDs in the reflection mode were diffused by a diffuser and brought onto focus by a convex lens and diverged by a concave lens. The scattered light was incident onto a beam splitter, from which half was reflected towards the sample, and the other half was transmitted

which was brought to focus by a convex lens towards the imager to be captured by the imager through the computer. Similarly, light from the LEDs in scattering mode is scattered by a diffuser and brought onto focus by a convex lens on the sample where the light is transmitted through the sample. The transmitted light is focused by a lens towards the imager to be detected and captured by the imager using the computer. Finally, in transmission mode, light from the LEDs is scattered by a diffuser and passed through a fibre to the ring from which it scattered around the sample stage before illuminating the sample. The transmitted light is brought to a focus by a lens after which it is detected by the imager and captured using the computer.

Multispectral images of the Giemsa stained thin blood smear slides were acquired using the multispectral light-emitting diode imaging microscope. The slides were numbered according to their blood type, and the day they were made.

The computer was switched on and launched onto the MATLAB algorithm, and the start bottom was turned on. The transmission mode was selected from the modes icon; the first slide was placed on the sample stage of the MSLEDIM. The 525 nm LED was chosen from under the transmission icon for focusing by adjusting the fine, coarse adjustment knobs interchangeably and the required gain and exposure time were set respectively. After the image has been focused, an image name was given to the sample image to the wavelength and the sample name and was saved into a folder (transmission file) by selecting the *write to file* icon. The wavelengths (13) were then selected one after the other and saved into the transmission file folder. A similar process was repeated for all other

slides. Two images were taken for each wavelength, and a total of twenty-six wavelength images were taken for each sample days. In all, a total of 234 wavelength images were obtained as shown in table 2.

Table 2: A distribution of the number of wavelength images taken for each blood sample

SAMPLES	IRBC-DAY 1	IRBC-DAY 6	UNINFECTED (URBCs)
AA	26 IMAGES	26 IMAGES	26 IMAGES
AS	26 IMAGES	26 IMAGES	26 IMAGES
SS	26 IMAGES	26 IMAGES	26 IMAGES

Images taken from the MSLEDIM were transferred into MATLAB application software from the folder in which all the images were. In MATLAB, pixel intensities for various red blood cells were obtained by drawing a rectangle around the individual RBCs to get their coordinates, as shown in Figure 10. The average intensities of the RBCs were then calculated from the pixel intensities retrieved and used for further analysis. Some of the information retrieved from MATLAB was exported to Microsoft Excel for further analysis.

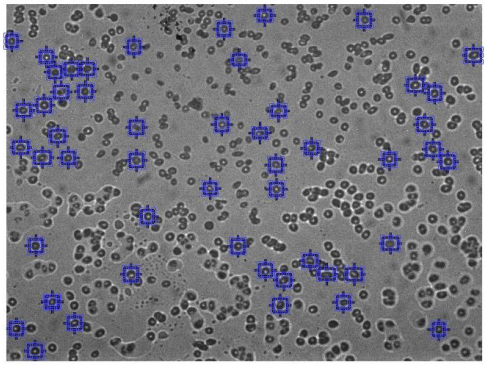

Figure 10: An image of red blood cells cropped for their pixel intensities.

Chapter Summary

This chapter describes the experimental methods and procedure for blood sample collection and protocol for culturing Plasmodium parasite into the blood samples. The final part of this chapter focuses on the description of the Multispectral Light Emitting Diode Imaging Microscope (MSLEDIM) system and procedure for acquiring multispectral images from the MSLEDIM.

CHAPTER FOUR

RESULTS AND DISCUSSION

Introduction

Results obtained from washing and culturing of the falciparum parasite in the blood sample is presented in the first section of this chapter, the second section presents the results, analysis and discussions of the multispectral images acquired using the multispectral light-emitting diode imaging microscope (MSLEDIM) in the transmission mode.

Results from washing and culturing of the falciparum parasite in the blood sample

Blood samples that were used for parasites culturing during the research were spun in a centrifuge; this process causes heavier elements in the blood sample to separate from the lighter elements. A specimen obtained after spinning is shown in Figure 11. Each spun gave three layers; where the bottom layer is the red blood cells (RBCs), the second layer is whitish (the buffy layer) and the third transparent layer is the blood plasma. The bottom layer, which is heaviest particulates in the blood is the erythrocytes which are the red blood cells (RBCs), while the buffy coat layer, is composed of the white blood cells and platelets. The blood plasma is made up of fluids which constitute water, proteins, nutrients, hormones etc. (Darmawan, 2019).

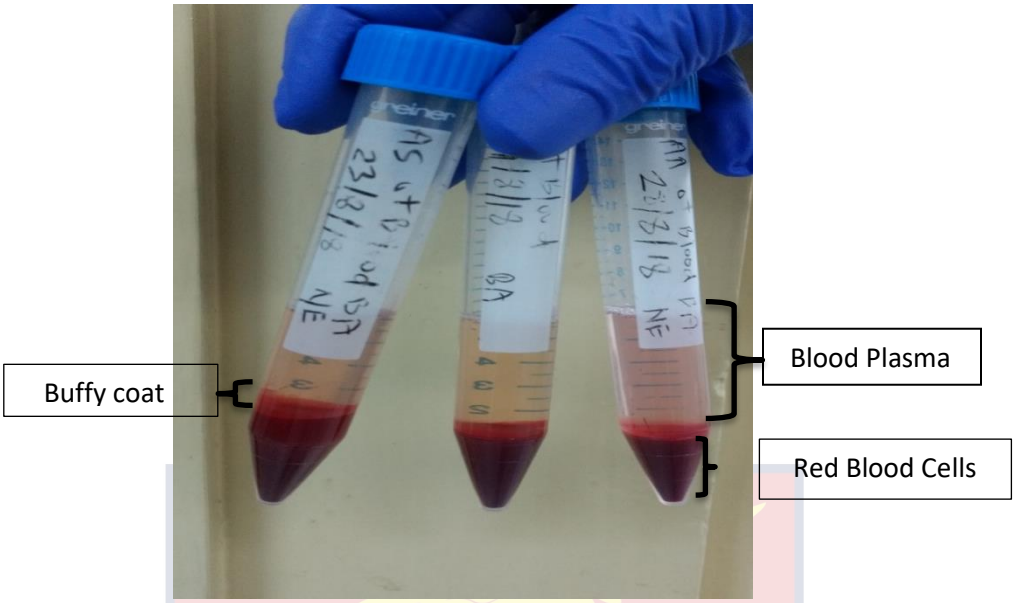

Figure 11: Three Blood samples after spinning showing Distinct layers: Bottom layer (erythrocytes/red blood cells (RBCs)), Middle layer (buffy coat/white blood cells (WBC's) and platelets) and Top layer (transparent medium/blood plasma).

Parasite synchronization was performed on the plasmodium parasites by subjecting them to sorbitol and percoll density centrifugations. Percoll synchronization purifies parasitized RBCs. After centrifugation, as shown in Figure 12, the upper layer comprises of dead cells and debris followed by the 35 % percoll layer. The lower layer contains enriched parasitized RBCs. The bottom layer, which is the 65 % percoll, mostly contains unparasitized RBCs and early-stage parasites. Repeating the synchronization process several times on the lower layer maximizes the recovery of several synchronized parasites, as shown in Figure 13.

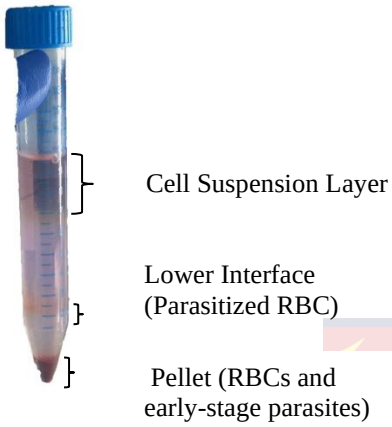

Figure 12: Parasitized RBCs after Percoll synchronization showing cell suspension layer (light pink), lower interface (pink) and pellet (RBCs (dark brown)).

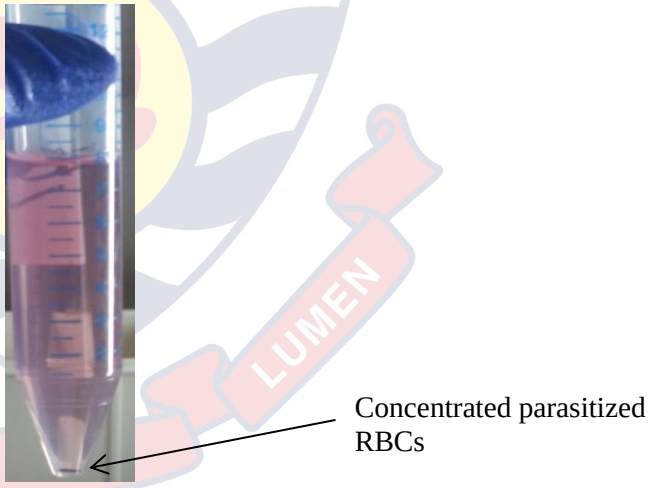

Figure 13: A centrifuged sample showing concentrated parasitized RBCs at the bottom

Figure 14: A well of blood samples (AA, AS and SS) infected with parasitized RBCs placed in a culture chamber.

Multispectral images acquired using the Multispectral Light Emitting Diode Imaging Microscope (MSLEDIM)

Thirteen multispectral images ranging from 370 nm to 940 nm of SS-IRBC-D1 obtained from the multispectral light-emitting diode imaging microscope (MSLEDIM) in transmission mode are as shown in Figure 15. Five each of the remaining samples images are shown in appendix A. It can be observed that SS-IRBC-D1 appear as dark grey spots in some of the bright images. From Figure 15, it can also be observed that some images (SS1_375 nm, SS1_525 nm and SS1_660 nm) appear darkest, which suggests that these images have a deficient transmission of these wavelengths. Images from wavelengths SS1_400 nm, SS1_470 nm, SS1_625 nm, SS1_850 nm, and SS1_940 nm appear much brighter. These images also suggest high transmission of these wavelengths. The remaining images (SS1_435 nm, SS1_590 nm, SS1_700 nm, SS1_750 nm and SS1_810 nm) can be adjudged as the brightest images obtained for the

sample. This result indicates that the transmission for these wavelengths from the sample to the imager was very high.

SS1_375 nm

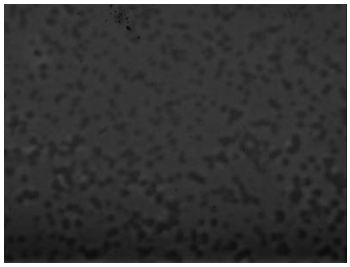

SS1_400 nm

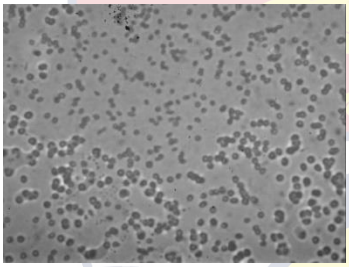

SS1_435 nm

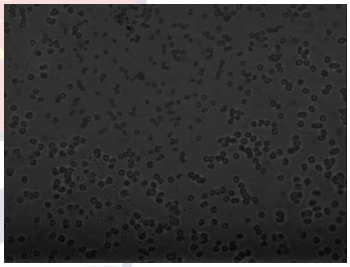

SS1_470 nm

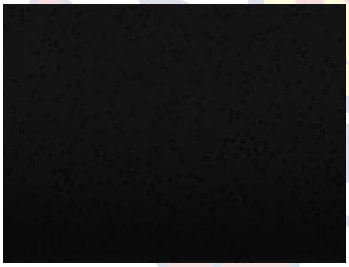

SS1_525 nm

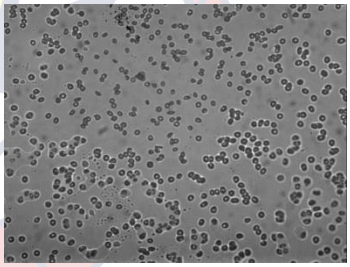

SS1_590 nm

SS1_625 nm

SS1_660 nm

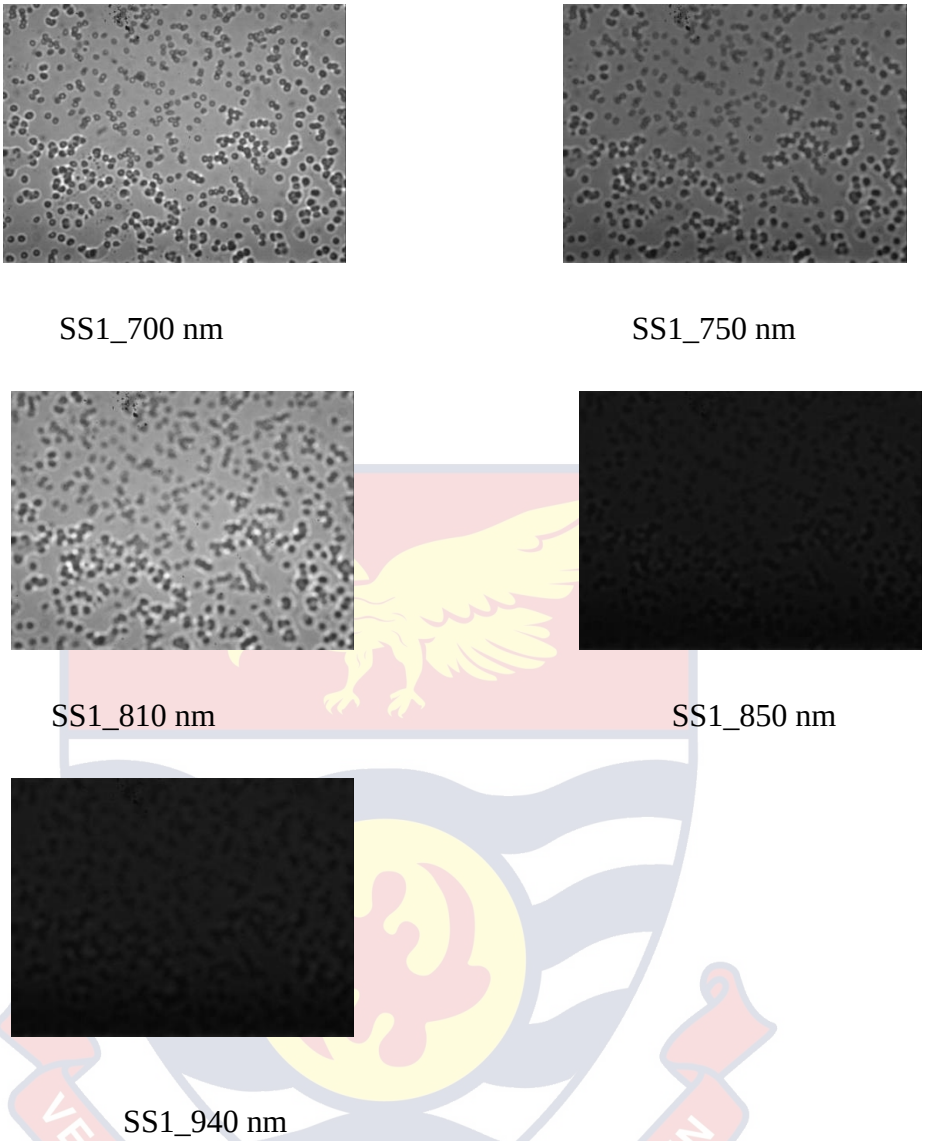

Figure 15: Thirteen Multispectral Transmission images from Wavelengths ranging from 375 nm to 940 nm of sickle cell SS-IRBC-D1 sample.

Average intensity values of RBCs (*Plasmodium*-infected (I) and uninfected (U)) extracted from greyscale images plotted against the wavelengths (13) for the various blood samples (AA-IRBC-D1, AA-IRBC-D6, AA-URBC, AS-IRBC-D1, AS-IRBC-D6, AS-URBC, SS-IRBC-D1, SS-IRBC-D6 and SS-URBC) are shown in Figures 16a, 16b, 17a, 17b, 18a and 18b.

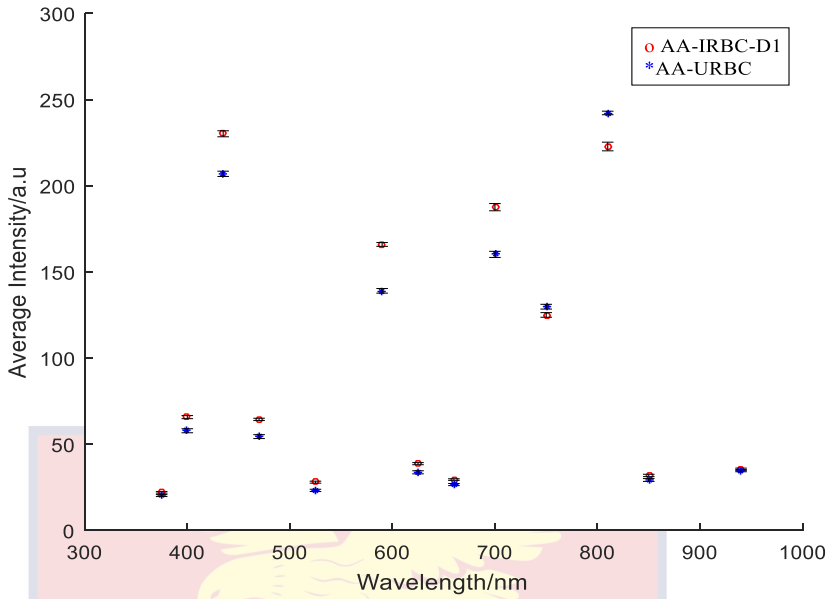

Figure 16a: A graph of Average Intensities of *Plasmodium*-infected "normal" Red Blood Cells (AA-IRBC-D1) (o) sample for day 1 and Uninfected Red Blood Cells (AA-URBC) (*) against Wavelengths (nm).

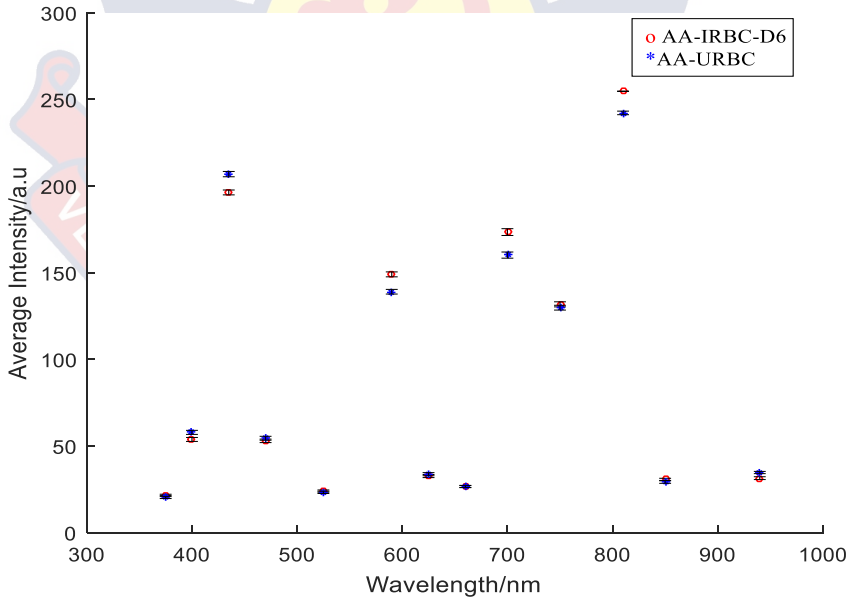

Figure 16b: Average Intensities of *Plasmodium*-infected "normal" Red Blood cells (AA-IRBC-D6) (o) sample for day 6 and Uninfected Red Blood Cells (AA-URBC) (*) against Wavelengths (nm).

Eight wavelengths from Figure 16a gave average intensity values below 100.0 au. The remaining wavelengths had an average intensity value above 100.0 au. Four wavelengths (435 nm, 590 nm, 700 nm and 810 nm) showed visible average intensity value differences between AA-IRBC-D1 and AA-URBC with a moderate intensity difference greater than 10.0 au. It can be observed that out of the four wavelengths, three have the average intensity of AA-IRBC-D1 to be greater than that of AA-URBC in accordance with literature (Opoku-Ansah et al., 2014) while one wavelength (810 nm) shows moderate intensity for AA-URBC to be greater than that of AA-IRBC-D1. This anomaly may be as a result of the property of the AA-IRBC-D1 cells which absorbed more light than AA-URBC.

Figure 16b shows a similar trend in average intensity distribution compared to Figure 16a, with smaller intensity differences between AA-IRBC-D6 and AA-URBC. In Figure 16b, three average intensities of AA-IRBC-D6 were lower than that of AA-URBC. This anomaly may be a property of the AA-IRBC-D6 cells which absorbed more light at these wavelengths (400 nm, 435 nm and 940 nm). Wavelengths with a remarkable average intensity difference of a value greater than 10.0 a.u in Figure 16a (435 nm, 590 nm and 700 nm) and 20.0 a.u in 16b (590 nm, 700 nm and 810 nm) were chosen as markers.

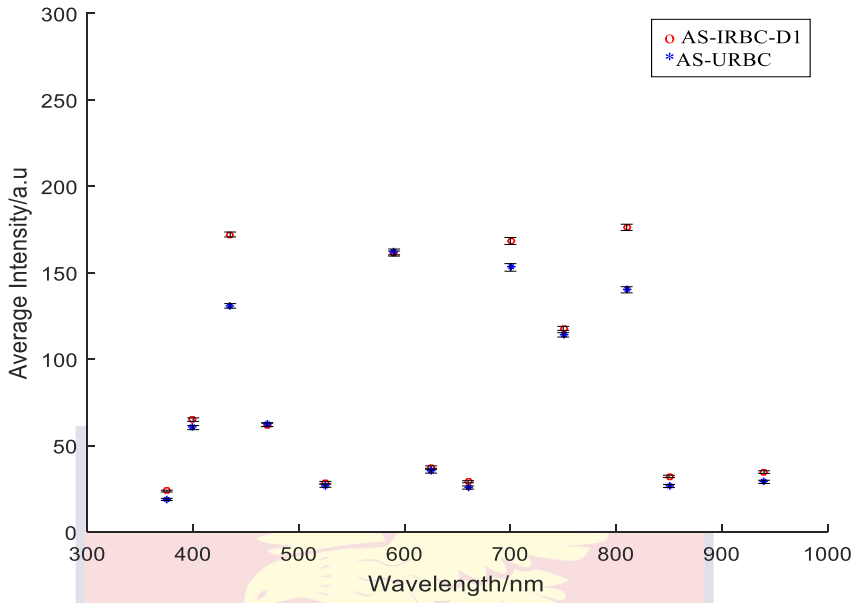

Figure 17a: Average Intensities of *Plasmodium*-infected Sickle Trait Red Blood Cells (AS-IRBC-D1) (o) sample for day 1 and Uninfected Red Blood Cells (AS-URBC) (*) against Wavelengths (nm).

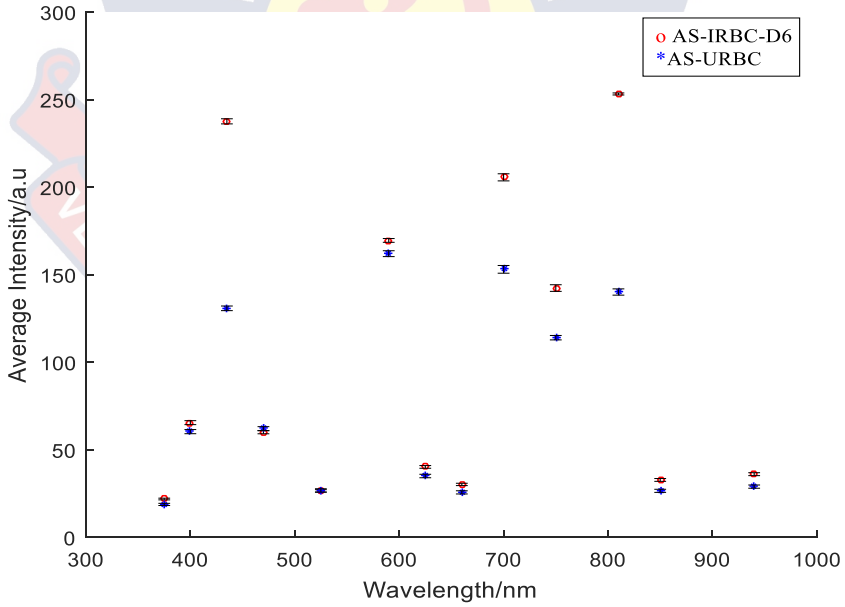

Figure 17b: Average Intensities of *Plasmodium*-infected Sickle Trait Red Blood Cells (AS-IRBC-D6) (o) sample for day 6 and Uninfected Red Blood Cells (AS-URBC) (*) against Wavelengths (nm).

From Figure 17a, eight wavelengths had average intensity value less than 100.0 a.u while the remaining wavelengths had average intensity above 100.0 au. Three wavelengths (435 nm, 700 nm and 810 nm), showed visible average intensity difference greater than 20.0 a.u between AS-IRBC-D1 and AS-URBC. Average intensity values obtained for these wavelengths were high, indicating high transmission and less absorption. Figure 17b shows similar average intensity distribution, as depicted in Figure 17a. The main difference being a substantial average intensity difference between AS-IRBC-D6 and AS-URBC for wavelength 750 nm. Thus Figure 17a and 17b had three (435 nm, 700 nm and 810 nm) and four (435 nm, 700 nm, 750 nm and 810 nm) wavelengths respectively being selected as markers.

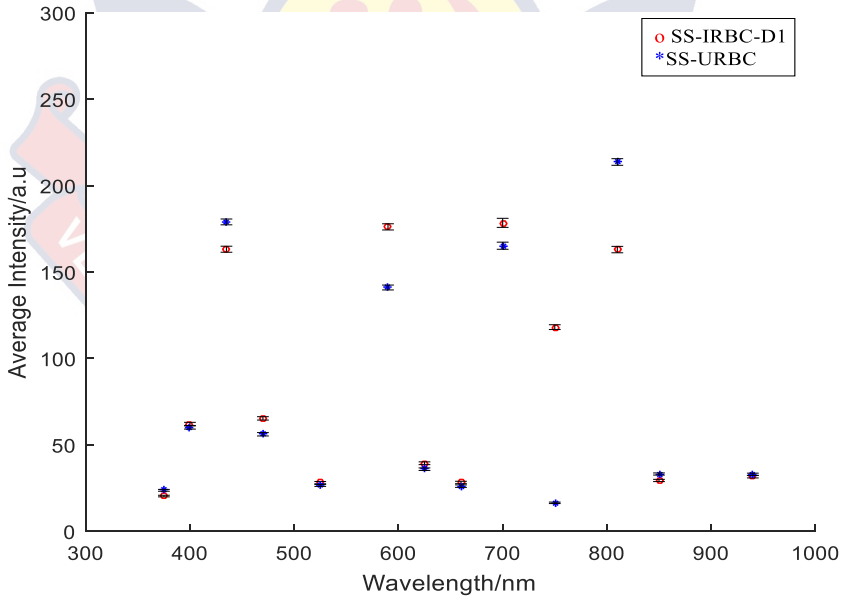

Figure 18a: Average Intensities of *Plasmodium*-infected Sickle Red Blood Cells (SS-IRBC-D1) (o) sample for day 1 and Uninfected Red Blood Cells (SS-URBC) (*) against Wavelengths (nm).

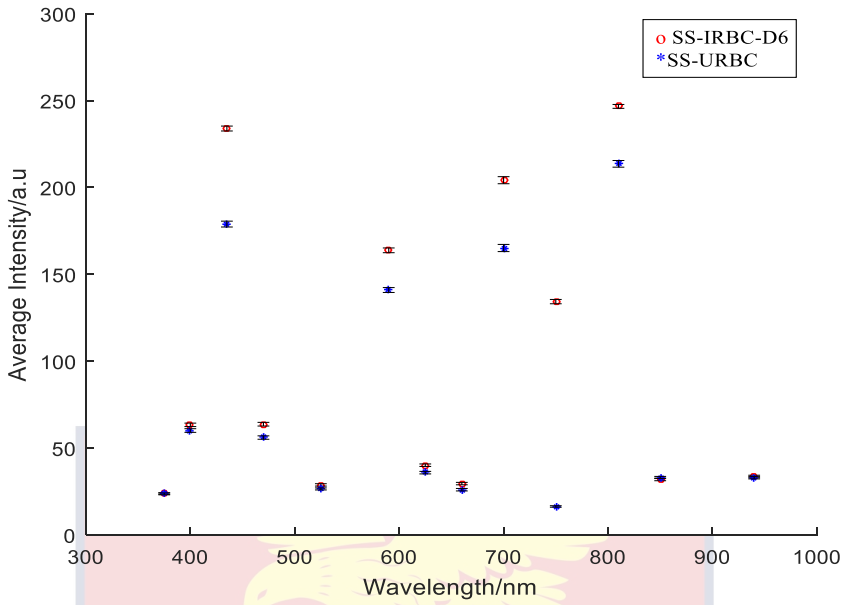

Figure 18b: Average Intensities of *Plasmodium*-infected Sickle Red Blood Cells (SS-IRBC-D6) (o) sample for day 6 and Uninfected Red Blood Cells (SS-URBC) (*) against Wavelengths (nm).

From Figure 18a, eight wavelengths gave average intensity values below 100.0 au. The remaining had intensity values above 100.0 au: with the wavelength 750 nm having an intensity value below 100.0 a.u for SS-URBC and intensity value greater than 100.0 a.u for SS-IRBC-D1. Five wavelengths (435 nm, 590 nm, 700 nm, 750 nm and 810 nm) showed visible average intensity value difference between SS-IRBC-D1 and SS-URBC with an intensity difference value greater than 20.0 au. However, it can be observed that out of the five wavelengths, two (435 nm and 810 nm) have intensity value of SS-URBC to be higher than SS-IRBC-D1. This anomaly is a property of the SS-IRBC-D1 cells which absorbed more light at these wavelengths.

Figure 18b depicts similar average intensity distribution, as shown in Figure 18a. The main difference being the intensity plot between SS-IRBC-D6

and SS-URBC for the wavelengths 435 nm and 810 nm. Thus Figure 18a and 18b had three (590 nm, 700 nm and 750 nm) and five (435 nm, 590 nm, 700 nm, 750 nm and 810 nm) wavelengths respectively being selected as markers.

Principal component analysis (PCA) was performed on the intensity data obtained from the images. This analysis was done to uncover the relationship among the observed variables and to buttress information on some wavelengths as markers. The eigenvalues of the principal components (PCs) contributing to the total variance of intensity values of the IRBCs and URBCs were represented. Figure 19 shows the result of a scree plot of 12 PCs which were obtained from the PCA. The PCA reduced the dimensionality of the variables, which are the intensity values at the various wavelengths. The plot was used to determine the number of PCs appropriate for discrimination and classification.

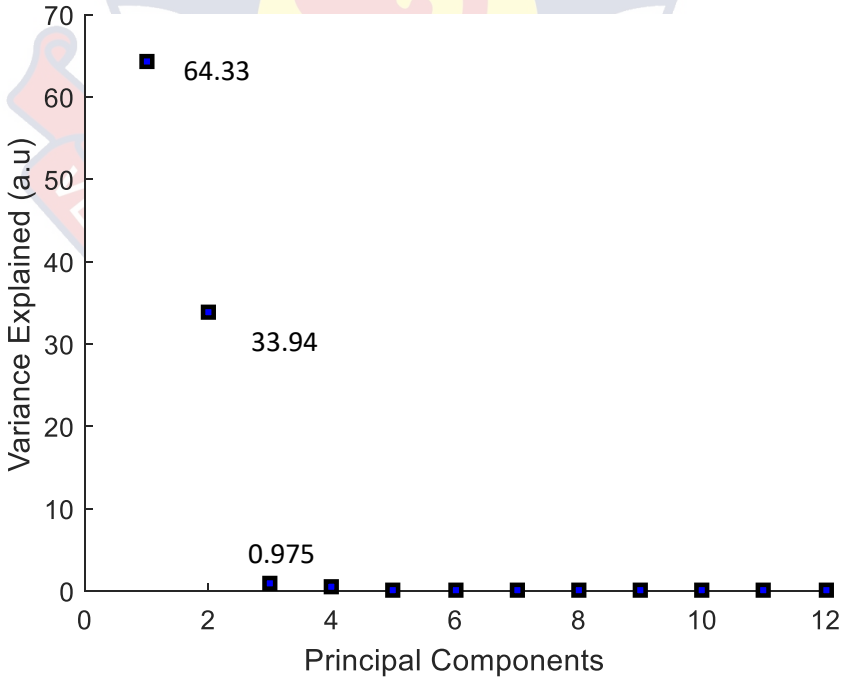

Figure 19: Scree plot showing the variance of the twelve principal components (PCs) involving the intensity values and wavelengths.

As suggested by Martinez and Martinez, the points before the curve levels off and becomes almost horizontal are the reasonable PCs (Martinez & Martinez, 2005). From Figure 19, the eigenvalues drop off rapidly after the third PC. This drop suggests that the first three PCs are suitable for analysis. It shows that the variances of the intensity data retained by all the twelve (12) PCs to ascertain the choice of the first three PCs. The first three PCs, which are PC1, PC2 and PC3 retained the maximum variance of the intensity data with 99.245 % cumulative variability. These were contributed by 64.33 % of PC1, 33.94 % for PC2 and 0.975 % for PC3 respectively.

The first two (2) PCs accounted for a high proportion of the variance; thus a 2-dimensional (2D) graphical representation of the data shows the scores which help in observing the trends, cluster and outlines of the data. The 2D plot also indicates that the chosen wavelengths are better for IRBCs and URBCs classification. Scatter plot of the first two principal components for these wavelengths was plotted.

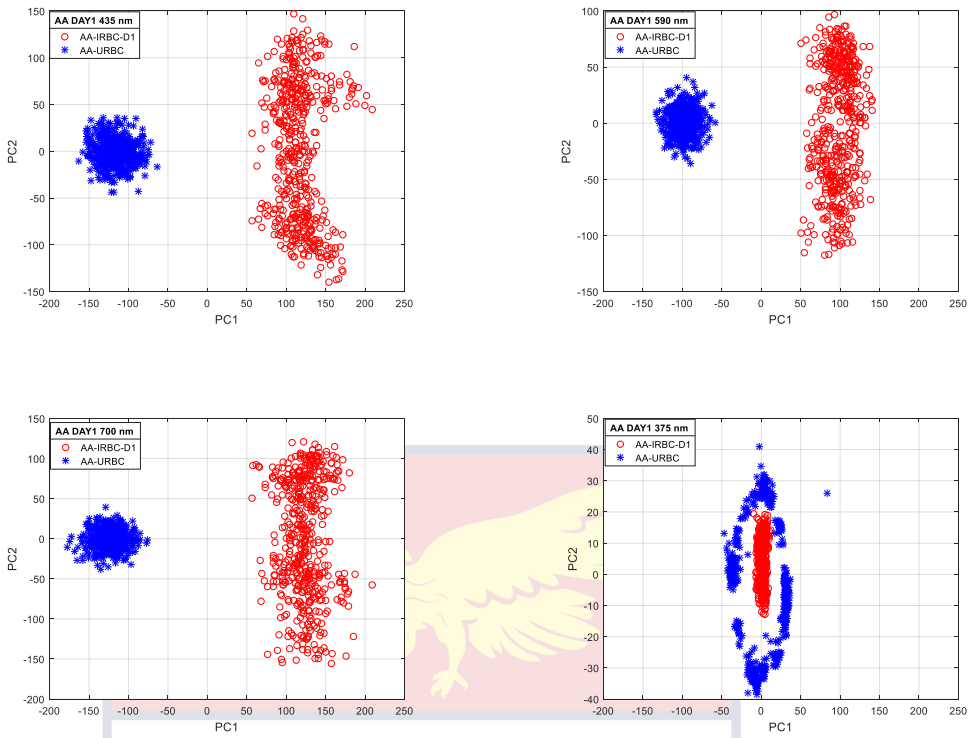

Figure 20: Scatter plot of the first two PCs of AA for day 1(AAD1) Blood Group, showing the *Plasmodium*-infected Red Blood Cells (AA-IRBC-D1) (⊙) and the Uninfected Red Blood Cells (AA-URBC) (*) of wavelengths 435 nm, 590 nm, 700 nm, 375 nm, respectively.

Figure 20 shows a significant separation between the coefficients AA-IRBC-D1 and AA-URBC at wavelengths 435 nm, 590 nm and 700 nm on the PC1 axis. In contrast, the wavelength 375 nm (which is a non-marker) did not show any distinct separation. It can be observed from the scatter plot at 435 nm, 590 nm and 700 nm that, the coefficients of AA-URBC are closely clustered whiles the coefficients of AA-IRBC-D1 are vertically spread. Also, AA-IRBC-D1 has positive PC1 coefficients which signify that it is positively correlated to PC1 extents AA-URBC is negatively related to the PC1 due to its negative coefficients.

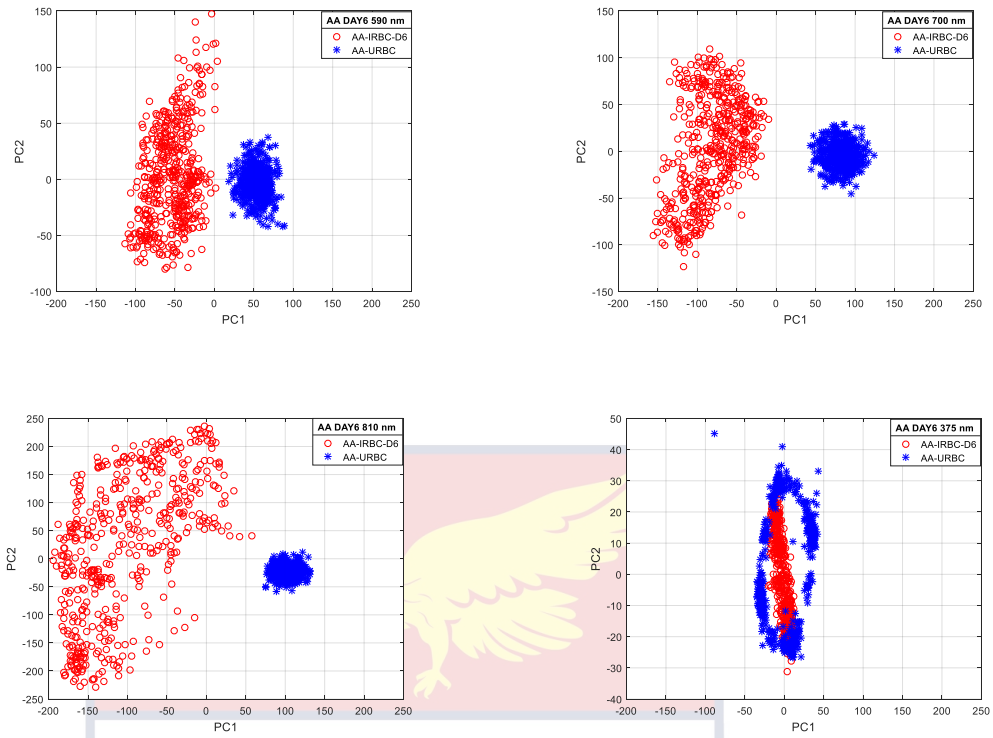

Figure 21: Scatter plot of the first two PCs of AA for day 6 (AAD6) Blood Group, showing the *Plasmodium*-infected Red Blood Cells (AA-IRBC-D6) (⊙) and the Uninfected Red Blood Cells (AA-URBC) (*) of Wavelengths 590 nm, 700 nm, 810 nm, 375 nm respectively.

Figure 21 shows a distinct separation between the coefficients AA-IRBC-D6 and AA-URBC at wavelengths 590 nm, 700 nm and 810 nm on the PC1 axis while the wavelength 375 nm (which is a non-marker) did not show any separation. It can be observed from the scatter plot at 590 nm, 700 nm and 810 nm that, the coefficients of AA-IRBC-D6 are closely clustered while the coefficients of AA-URBC are vertically spread. Also, AA-URBC has positive PC1 coefficients whiles AA-IRBC-D6 is negatively correlated to the PC1.

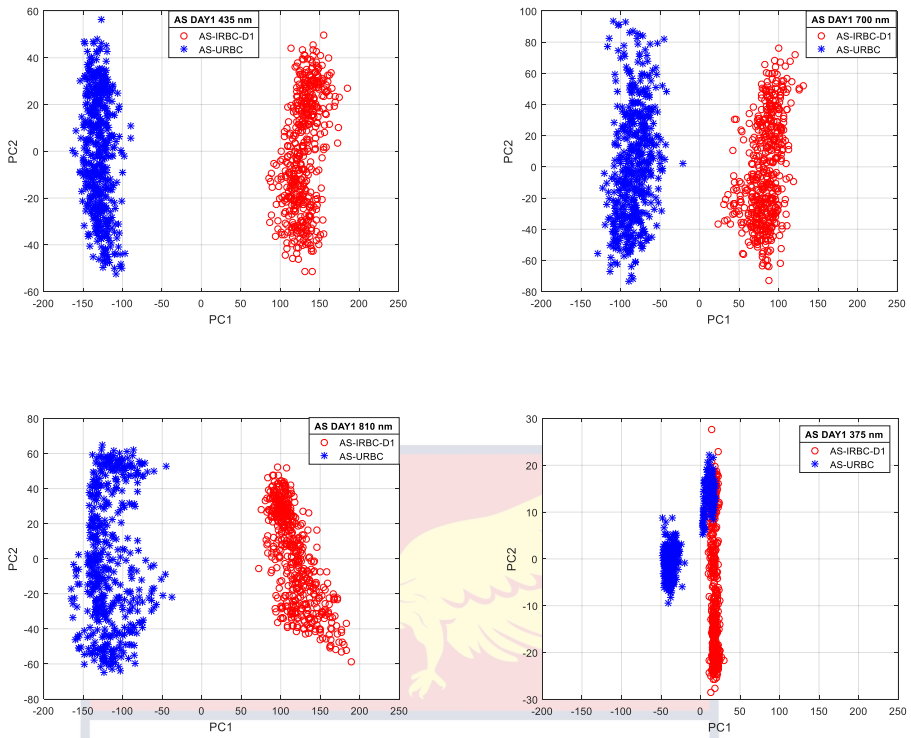

Figure 22: Scatter plot of the first two PCs of AS for day 1 (ASD1) Blood Group, showing the *Plasmodium*-infected Sickle Red Blood Cells (AA-IRBC-D1) (⊙) and the uninfected red blood cells (AS-URBCs) (*) for the wavelengths 435 nm, 700 nm, 810 nm and 375 nm respectively.

From Figure 22, a distinct separation between the coefficients AS-IRBC-D1 and AS-URBC from the scatter plot at wavelengths 435 nm, 700 nm and 810 nm can be observed on the PC1 axis. The scatter plot at wavelength 375 nm (which is a non-marker) did not show any separation with some coefficients of AS-URBC being imbricated in AS-IRBC-D1 coefficients. It can be observed from the scatter plot at 435 nm, 700 nm and 810 nm that, the coefficients for both AS-IRBC-D1 and AS-URBC are vertically spread.

Also, AS-IRBC-D1 has positive PC1 coefficients whiles is AS-URBC negatively correlated to the PC1.

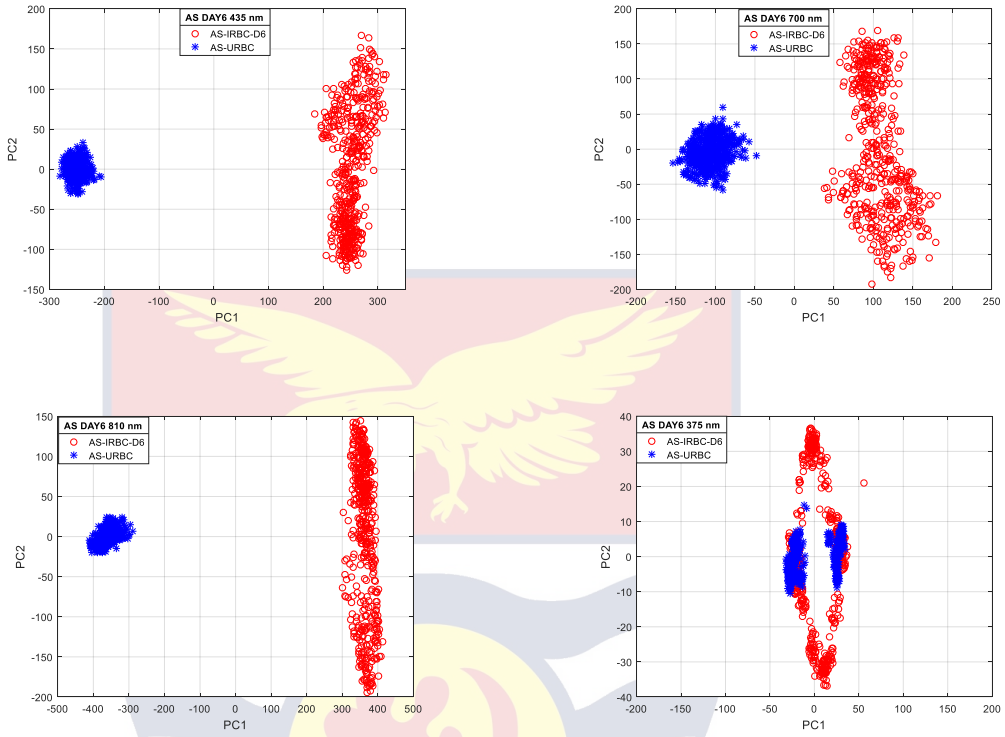

Figure 23: Scatter plot of the first two PCs of AS for day 6 (ASD6) Blood Group, showing the *Plasmodium*-infected Sickle Red Blood Cell (AS-IRBC-D6) (⊙) and the Uninfected Red Blood Cells (AS-URBC) (*) for the wavelengths 435 nm, 700 nm, 810 nm and 375 nm.

Figure 23 shows a distinct separation between the coefficients AS-IRBC-D6 and AS-URBC from the scatter plot at wavelengths 435 nm, 700 nm and 810 nm can be observed on the PC1 axis. The scatter plot at wavelength 375 nm (which is a non-marker) did not show any separation: with the coefficients of AS-URBC being imbricated in AS-IRBC-D6 coefficients. It can be observed from the scatter plot at 435 nm, 700 nm and 810 nm that, the coefficients for AS-IRBC-D6 are vertically spread, and the coefficients of

AS-URBC are closely clustered. Also, AS-IRBC-D6 is positively correlated to PC1 while AS-URBC is negatively related to the PC1.

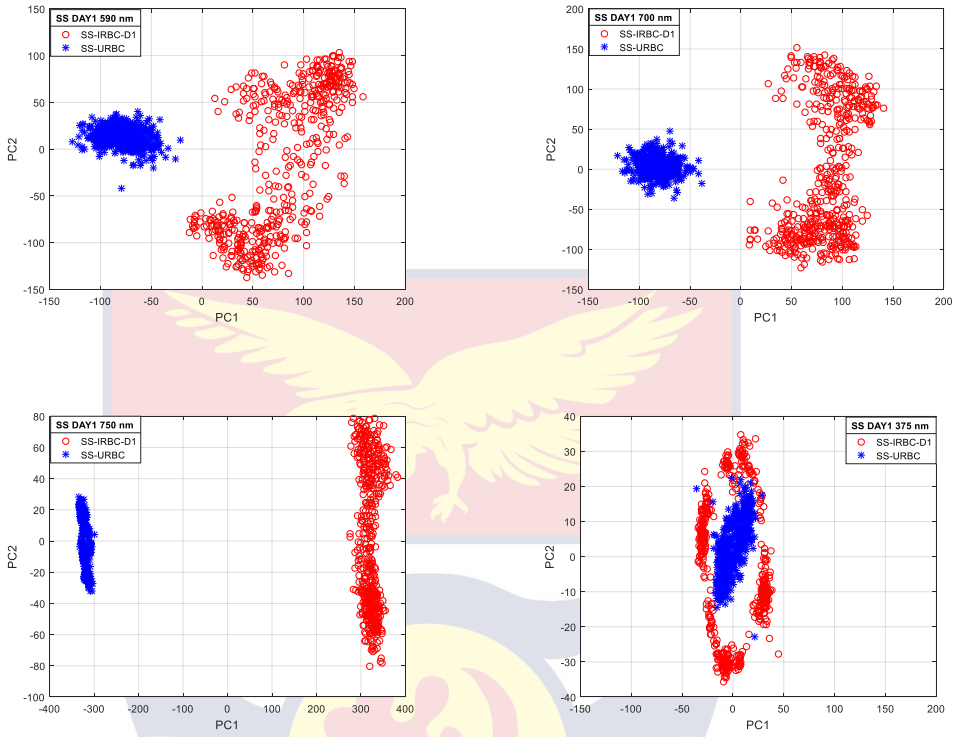

Figure 24: Scatter plot of the first two PCs of SS for day 1 (SSD1) Blood Group, showing the *Plasmodium*-infected Sickle Red Blood Cells (SS-IRBC-D1) (o) and the Uninfected Red Blood Cells (SS-URBCs) (*) for the wavelengths 590 nm, 700 nm, 750 nm and 375 nm respectively.

A distinct separation between the coefficients SS-IRBC-D1 and SS-URBC at wavelengths 590 nm, 700 nm and 750 nm on the PC1 axis can be observed in Figure 24. The scatter plot at wavelength 375 nm (which is a non-marker) did not show any separation: with the coefficients of SS-URBC being embedded in SS-IRBC-D1 coefficients. It can be observed from the scatter plot of SS-URBC that, at 590 nm, 700 nm and 750 nm the coefficients of are closely clustered

whiles the coefficients SS-IRBC-D1 are vertically spread. Also, SS-IRBC-D1 is positively correlated to PC1 while is SS-URBC is negatively related to the PC1.

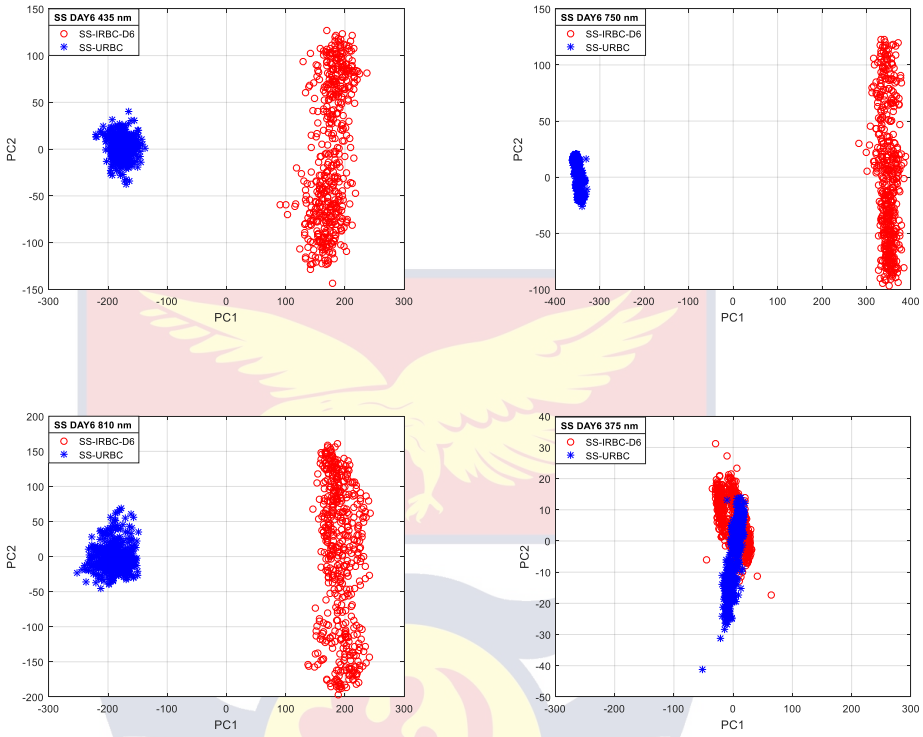

Figure 25: Scatter plot of the first three PCs of SS for day 6 (SSD6) Blood Groups, showing the Plasmodium-infected Sickle Red Blood Cells (SS-IRBC-D6) (⊙) and the Uninfected Red Blood Cells (SS-URBC) (*) for the Wavelengths 435 nm, 750 nm, 810 nm and 375 nm respectively.

Figure 25 shows a significant separation between the coefficients SS-IRBC-D6 and SS-URBC from the scatter plot at wavelengths 435 nm, 750 nm and 810 nm can be observed on the PC1 axis. The scatter plot at wavelength 375 nm (which is a non-marker) did not show any separation: with the coefficients of SS-URBC overlapping SS-IRBC-D6 coefficients. It can be observed from the scatter plot at 435 nm, 750 nm and 810 nm that, the

coefficients for SS-IRBC-D1 are vertically spread, and the coefficients of SS-URBC are closely clustered. Also, SS-IRBC-D6 is positively correlated to PC1 while SS-URBC is negatively related to the PC1.

Table 3: A table showing the wavelength markers of the samples

WAVELENGTH MARKERS (nm)	SAMPLES					
	AAD1	AAD6	ASD1	ASD6	SSD1	SSD6
435	✓	✓	✓	✓		✓
590	✓	✓			✓	✓
700	✓		✓	✓	✓	✓
750				✓	✓	✓
810		✓	✓	✓		✓

Two common sickle cell blood groups: AS (sickle cell trait) and SS (sickle cell disease) while (AA which serves as a control), were used for this research. From Table 3, it could be observed that the wavelength markers for AAD1 and AAD6 have the same wavelengths (590 nm and 700 nm) as markers. AAD1 has 435 nm as a marker whiles AAD6 does not. A similar observation could be made for AAD6 having 810 nm as a marker while AAD1 does not. The difference in the wavelength marker may be due to the increase of parasite in the blood

samples. It can be said that, as the days increase, there was also an increase in the plasmodium parasites, causing the infected blood sample to behave differently as it was in day1. A similar observation can be made for all the other blood samples. The wavelength markers obtained for AS blood group is quite similar for both day1 (D1) and day6 (D6) excluding the wavelength 750 nm, which was for ASD6. It can also be observed that the wavelength marker for ASD6 is quite similar to that of the SS blood group. Even though sickle cell trait (AS) is highly protective against malaria during its infection period, as the days of infection increase, the blood group AS in D6 starts to behave as the SS blood group. The wavelength markers for the SS blood were also found to be different with SSD1 having the wavelengths 590 nm, 700 nm and 750 nm while SSD6 had 435 nm, 590 nm, 700 nm, 750 nm and 810 nm as markers.

The use of MSLEDIM in transmission mode to classify red blood cells infected with malaria is research conducted by Opoku-Ansah and results obtained revealed wavelengths 435 nm and 660 nm as markers for classifying IRBCs and URBCs. The wavelength for classification from Opoku-Ansah was the same through-out whiles in this research, the markers varied as observed in Table 3. This distinction can be attributed to the fact that Opoku-Ansah's research was done *in vivo* while this research was done *in vitro.* A recent study indicates that the condition parasites experience in their natural states (in vivo) is different from the condition they experience when they are cultured (*in vitro)* (LeRoux, Lakshmanan, & Daily, 2009). Even though sickle cell and sickle trait RBC has some resistance to the plasmodium parasite, an inference can be drawn stating

that wavelength provided in Table 3 can be used in the determination of the various sickle cell groups in respect to the day of infection.

Chapter summary

Using extracted average pixel intensities and PCA, this chapter analyzed and discussed results obtained from grayscale multispectral images using the multispectral light-emitting diode imaging microscope system.

CHAPTER FIVE

SUMMARY, CONCLUSIONS AND RECOMMENDATIONS

Overview

The summary and conclusions from the thesis are presented in the first part of this chapter whiles recommendations for future work are shown in the last part of this chapter.

Summary

In summary, chapter one provided an overview of sickle cell anaemia and malaria and their various modes of diagnosis. The background to multispectral imaging technique, the scope of work and organization of the study was also included. Chapter two reviewed the literature on spectroscopy with emphasis on multispectral imaging. In addition the chapter provided a review on multivariate data analysis techniques and sickle cell disease. Chapter three described the experimental methods and procedure for blood sample collection, protocol for culturing Plasmodium parasite into the blood samples and the description of the Multispectral Light Emitting Diode Imaging Microscope (MSLEDIM) system and the procedure for acquiring multispectral images from the MSLEDIM. Chapter four utilized multispectral imaging techniques in combination with multivariate analysis (PCA) to detect and discriminate sickle red blood cell infected with malaria parasites. The multispectral images were acquired in transmission mode. In all five wavelengths were found to be markers for discriminating sickle IRBC's and Sickle URBC's.

Conclusions

Employing the MSLEDI microscopy technique in the transmission mode, it has been possible to discriminate malaria-infected and uninfected sickle red blood cell. Using extracted average pixel intensities from grayscale multispectral images, five wavelengths in all consisting (435 nm, 590 nm, 700 nm, 750 nm and 810 nm) were found to be markers for discriminating sickle IRBC and sickle URBC. The wavelength (700 nm) was a standard marker for determining infected, and uninfected blood groups (AA, AS and SS) infected with the malaria parasite. Three wavelengths (435 nm, 590 nm and 700 nm) were found as markers for AAD1 whilst 590 nm, 700 nm and 810 nm were markers found for AAD6. Also, the wavelength (435 nm, 700 nm and 810 nm) and (435 nm, 700 nm, 750 nm and 810 nm) were markers found for ASD1 and ASD6 respectively. Finally, the spectral bands (590 nm, 700 nm and 750 nm) were markers found for the blood group SSD1 and (435 nm, 590 nm, 700 nm, 750 nm and 810 nm) for the blood group SSD6. Upon further analysis with PCA, two PCs confirmed these five wavelengths as markers for discriminating sickle IRBC and sickle URBC. This study shows that a sickle cell blood infected with malaria could be distinguished using the wavelength marker Multispectral Light Emitting Diode Imaging Microscope (MSLEDIM).

Recommendations

It is recommended that other optical spectroscopic techniques such as Laser-induced Fluorescence (LIF) and Raman spectroscopy be employed to study and characterize sickle red blood cell infected with malaria. It is also

recommended that the MSI technique be applied to other blood disorders such as normocytic anaemia, haemolytic anaemia, fanconi anaemia and pernicious anaemia.

REFERENCES

Adueming, P. , Eghan, M. , Anderson, B. , Kyei, S. , Opoku-Ansah, J. , Amuah, C., Sackey, S. & Buah-Bassuah, P. (2017) Multispectral imaging in combination with multivariate analysis discriminates selenite induced cataractous lenses from healthy lenses of sprague-dawley rats. Open Journal of Biophysics, **7**, 145-156. doi: 10.4236/ojbiphy.2017.73011

Agbana, T. E., Diehl, J. C., Van Pul, F., Khan, S. M., Patlan, V., Verhaegen, M., & Vdovin, G. (2018). Imaging & identification of malaria parasites using cellphone microscope with a ball lens. PLoS ONE, 13(10), 1–15. https://doi.org/10.1371/journal.pone.0205020

Albregtsen, F. (2008). 2 Reflection, refraction, diffraction, and scattering. 1–82. Retrieved January 5, 2018 from https://www.uio.no/ studier/emner/ matnat/ifi/INF-GEO4310/h09/undervisningsmateriale/imaging-kap2.pdf

Alkrimi, J. A., Tome, S. A., & George, L. E. (2019). Classification of red blood cells using principal component analysis technique. European Journal of Engineering Research and Science, 4(2), 17–22

Ballas, S. K., Lieff, S., Benjamin, L. J., Dampier, C. D., Heeney, M. M., Hoppe, C., ... & Telen, M. J. (2010). Definitions of the phenotypic manifestations of sickle cell disease. American journal of hematology, 85(1), 6-13

Bohren, C. F., & Huffman, D. R. (1983). Absorption and scattering of light by small particles (1st Editio; JOHN WILEY & SONS, Ed.). New York: A Wiley-Interscience Publication

Chotivanich, K., Silamut, K., & Day, N. P. J. (2007). Laboratory diagnosis of malaria infection - A short review of methods. New Zealand Journal of Medical Laboratory Science, 61(1), 4–7

Instituto Gulbenkian de Ciencia. (2011, April 29). Mystery solved: How sickle hemoglobin protects against malaria. ScienceDaily. Retrieved May 21, 2018 from www.sciencedaily.com/releases/2011/04/110428123931.html

Coffey, V. C. (2012). Multispectral imaging moves into the mainstream. Optics and Photonics News, 23(4), 18-24

Cones, C. (1996). Visible Light and the eye's response Retrieved January 5, 2017 from https://www.physicsclassroom.com/class/light/Lesson-2/Visible-Light-and-the-Eye-s-Response

Darmawan, D. (2019). Blood composition and functions. Journal of Chemical Information and Modeling, 53(9), 1689–1699 https://doi.org/10.1017/CBO9781107415324.004

Davidson, M. W., & Abramowitz, M. (2002). Optical microscopy. Encyclopedia of imaging science and technology

Dolloff, N. G., & El-Deiry, W. S. (2009). Optical imaging. Introduction to the Science of medical imaging, 9780521747, 172–182. https://doi.org/10 .1017/CBO9780511994685.009

Ferrer-Galindo, L., Sañu-Ginarte, A. D., Fleitas-Salazar, N., Ferrer-Moreno, L. A., Rosas, R. A., Pedroza-Montero, M., & Riera, R. (2018). Denoising and principal component analysis of amplified raman spectra from red blood cells with added silver nanoparticles. Journal of Nanomaterials, 2018. https://doi.org/10.1155/2018/9417819

Fischer, C., & Kakoulli, I. (2006). Multispectral and hyperspectral imaging technologies in conservation: current research and potential applications. Studies in Conservation, 51(sup1), 3-16

Freeman, J., Downs, F., Marcucci, L., Lewis, E. N., Blume, B., & Rish, J. (1997, October). Multispectral and hyperspectral imaging: applications for medical and surgical diagnostics. In Proceedings of the 19th Annual International Conference of the IEEE Engineering in Medicine and Biology Society.'Magnificent Milestones and Emerging Opportunities in Medical Engineering'(Cat. No. 97CH36136) (Vol. 2, pp. 700-701). IEEE

Friedman, M. J. (1978). Erythrocytic mechanism of sickle cell resistance to malaria. Proceedings of the National Academy of Sciences, 75(4), 1994-1997

Gauglitz, E. G. (2003). Handbook of Spectroscopy near-infrared spectroscopy Handbook of Analytical Techniques In-situ Spectroscopy in Heterogeneous Catalysis

GIS Geography. (2015). Multispectral vs Hyperspectral imagery explained What's the difference between multispectral vs hyperspectral imagery ? 1–5. Retrieved July 20,2017 from https://gisgeography.com/open-source-remote-sensing-software-packages

Gupta, S., Ghosh, N., & Banerjee, A. (2015). Reflection and refraction. Wave Optics, 37–51. https://doi.org/10.1201/b19330-4

Henderson, T. (2015). Light waves and color. Retrieved November 6, 2017, from https://www.physicsclassroom.com/class/light/Lesson-2/Visible-Light-and-the-Eye-s-Response

Hong, X. U., & Xiang, W. (2020). Applications of multispectral / hyperspectral imaging technologies in military. CNKI JOURNAL, 9–11

Mayo clinic, Sickle cell anemia. Retrieved October 7, 2018 from https://www.mayoclinic.org/diseases-conditions/sickle-cell-anemia

Indies, W. (2019). Mortality from sickle cell disease in Africa. 330(7489), 432–433. https://doi.org/10.1136/bmj.330.7489.432

Inusa, B. P., Hsu, L. L., Kohli, N., Patel, A., Ominu-Evbota, K., Anie, K. A., & Atoyebi, W. (2019). Sickle cell disease—genetics, pathophysiology, clinical presentation and treatment. International Journal of Neonatal Screening, 5(2), 20

Javidi, B., Markman, A., Rawat, S., O'Connor, T., Anand, A., & Andemariam, B. (2018). Sickle cell disease diagnosis based on spatio-temporal cell dynamics analysis using 3D printed shearing digital holographic microscopy. Optics express, 26(10), 13614-13627. https://doi.org/10.1364/oe.26.013614

Jianwei, Q., Kuanglin, C., Moon, S. K., Renfu, L., & Thomas, F. B. (2013). Hyperspectral and multispectral imaging for evaluating food safety and quality. Science Direct, 1–3. https://doi.org/10.1016/j.jfoodeng.2013.04.001

Kanchanawong, P. (2017). Sickle cell disease. Retrieved November 8, 2018 from National University of Singapore and National Heart, Lung and blood Institute. website: https://www.nhlbi.nih.gov/health/health-topics/topics/sca

Ogendal, L. (2016). Light Scattering a brief introduction. University of Copenhagen: Copenhagen, Denmark

LeRoux, M., Lakshmanan, V., & Daily, J. P. (2009). Plasmodium falciparum biology: analysis of in vitro versus in vivo growth conditions. Trends in Parasitology, 25(10), 474–481. https://doi.org/10.1016/j.pt.2009.07.005

Makani, J., Cox, S. E., Soka, D., Komba, A. N., Oruo, J., Mwamtemi, H., ... & Newton, C. R. (2011). Mortality in sickle cell anemia in Africa: a prospective cohort study in Tanzania. PloS one, 6(2), e14699

Mansouri, A., Marzani, F. S., & Gouton, P. (2005, September). Neural networks in two cascade algorithms for spectral reflectance reconstruction. In IEEE International Conference on Image Processing 2005 (Vol. 2, pp. II-718). IEEE.https://doi.org/10.1109/ICIP.2005.1530156

Nelson, S. A. (2014). monochromatic light. Retrieved December 3, 2018 from https://www.tulane.edu/~sanelson/eens211/proplight.htm

Nonell, S., & Viappiani, C. (2008). Basic spectroscopy. Retrieved February 3, 2017 from http://photobiology.info/Nonell_Viappiani.html. 1–24

Ogedegbe, H. O. (2002). Sickle cell disease: an overview. Laboratory medicine, 33(7), 515-543

Opoku-Ansah, J., Eghan, M. J., Anderson, B., & Boampong, J. N. (2014). Wavelength markers for malaria (Plasmodium Falciparum) infected and uninfected red blood cells for ring and trophozoite stages. Applied Physics Research, 6(2), 47–55. https://doi.org/10.5539/apr.v6n2p47.

Payne, D. (1988). Use and limitations of light microscopy for diagnosing malaria at the primary health care level. Bulletin of the World Health Organization, 66(5), 621–626

Pūtaiao, P. A. (2012). Reflection of light. 1–11. Retrieved March 15, 2018 from www.sciencelearn.org.nz

Robert, A., Henny, B., Kenneth, I. A., Carine, B., Harold, B., Kenneth, B., … Oswaldo, C. (2002). The management of sickle cell disease. In National Institutes of Health, National Heart, Lung, and Blood Institute (Fourth edi). Maryland: NIH PUBLICATION

Salmani Manjunath, P., Mindolli, P. B., & Peerapur, B. V. (2011). Comparative study of peripheral blood smear and quantitative buffy coat in malaria diagnosis. *Journal of Communicable Diseases*, *43*(1), 57–59. https://doi.org/10.4103/0377

Smith, L. I. (2002). A tutorial on principal components analysis introduction

Spread, P. (2019). Resolution microscopyU. Retrieved November 27,2019 From https://www.microscopyu.com/microscopy-basics/resolution.

Svanberg, S. (2003). Atomic and molecular spectroscopy. Springer-Verlag. https://doi.org/10.1007/978-642-18520-5

Tangpukdee, N., Duangdee, C., Wilairatana, P., & Krudsood, S. (2009). Malaria diagnosis: A brief review. Korean Journal of Parasitology, 47(2), 93–102. https://doi.org/10.3347/kjp.2009.47.2.93

Tidy, C. (2015). Sickle cell disease and sickle cell anaemia. Am J Med, 1–8.

Vander Voort, G. F. (2005). Optical microscopy. Encyclopedia of Condensed Matter Physics, 175–182. https://doi.org/10.1016/B0-12-369401-9/00579-9.

W.H.O. (2018). Sickle Cell Disease. Retrieved September 20, 2018, from World Health Organisation website: https://www.afro.who.int/health-topics/sickle-cell-disease

Warhurst, D. C., & William, J. E. (1996). Laboratory diagnosis of malaria. ACP Broadsheet No 148, 22(4), 448–451. https://doi.org/10.1177/0093854895022004009

Weyland, M., Chen, Z., D'Alfonso, A., Zhu, Y., Medhekar, N., Dwyer, C., . . . Allen, L. (2016). Making every electron count: Materials characterization by quantitative analytical scanning transmission electron microscopy. Microscopy and Microanalysis, 22(S3), 1430-1431. doi:10.1017/S1431927616007996

Wilkie, D. J., Gallo, A. M., Yao, Y., Molokie, R. E., Stahl, C., Hershberger, P. E., ... & Thompson, A. A. (2013). Reproductive health choices for young adults with sickle cell disease or trait: randomized controlled trial immediate posttest effects. Nursing research, 62(5),352 https://doi.org/10.1097/NNR.0b013e3182a0316b

Williams, I. Y. (2017). Types of Sickle Cell Disease. Retrieved August 13, 2020, from Sickle Cell Association of the National Capital Area, INC website: http://scancainc.org/learn/types-of-sickle-cell-disease

Williams, T. N., & Thein, S. L. (2018). Sickle cell anemia and Its phenotypes. Annual Review of Genomics and Human Genetics, 19, 113–147. https://doi.org/https://doi.org/10.1146/annurev-genom-083117-021320

Willoughby, C. T., Folkman, M. A., & Figueroa, M. A. (1996, January). Application of hyperspectral-imaging spectrometer systems to industrial inspection. In three-dimensional and unconventional imaging for industrial inspection and metrology (Vol. 2599, pp. 264-272). International Society for Optics and Photonics

Xu, R. (2002). Light Scattering: The background information. Particle characterization: Light scattering methods, 56-110. https://doi.org/https://doi.org/10.1007/0-306-47124-8_2

Zhang, C., Hou, C., Wang, X. X., Wang, Z. Z., Xu, W., Mulligan, J., … Liang, X. (2012). StitcHD final report. Encyclopedia of Computer Vision, 34(5), 14. https://doi.org/10.1007/978-0-387-31439-6

zumadahl, S. (2007). Visible light spectroscopy preparation. In Chemical Principles (6th edition, pp. 1–1073). https://doi.org/061894690X

APPENDICES

APPENDIX A: MULTISPECTRAL TRANSMISSION IMAGES FROM WAVELENGTHS OF AA, AS AND SS BLOOD SAMPLES

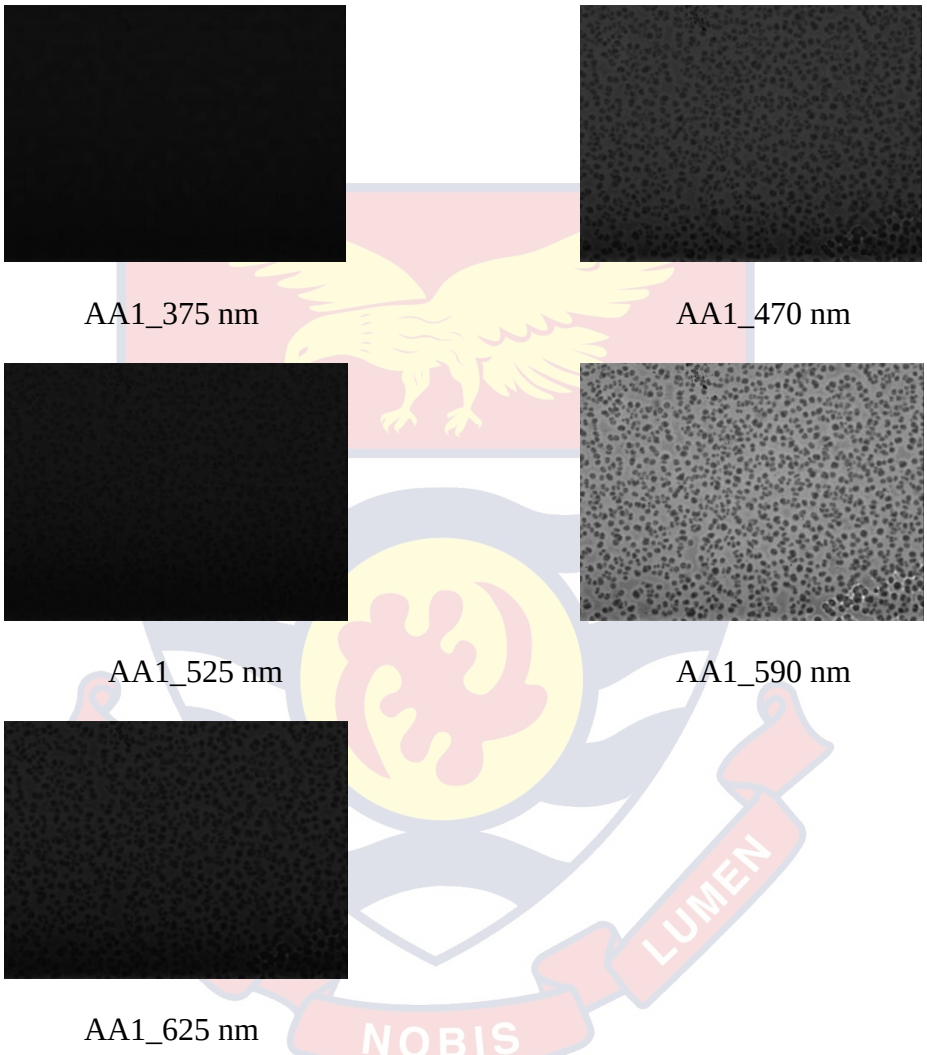

AA1_375 nm AA1_470 nm

AA1_525 nm AA1_590 nm

AA1_625 nm

Appendix A1: Five Multispectral images of AA-IRBC-D1 Sample.

AA6_375 nm

AA6_400 nm

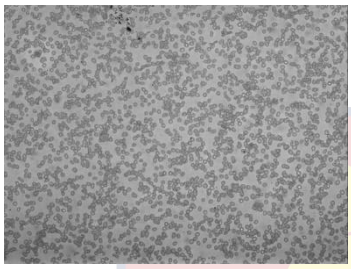

AA6_435 nm

AA6_470 nm

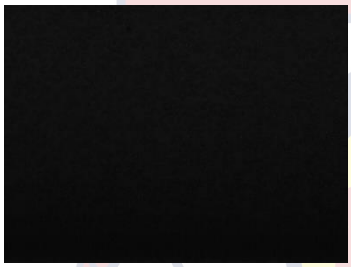

AA6_525 nm

Appendix A2: Five Multispectral images of AA-IRBC-D6 Sample.

AAU_375 nm

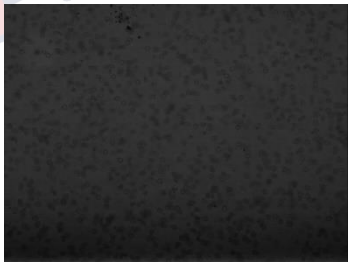

AAU_400 nm

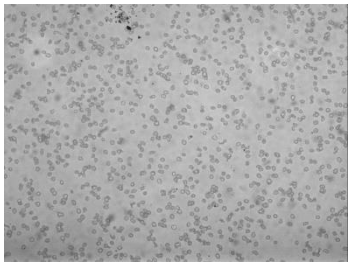

AAU_435 nm

AAU_470 nm

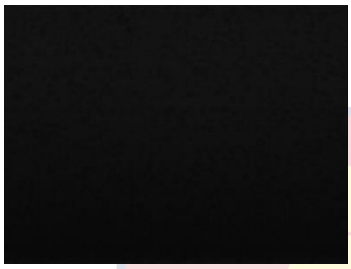

AAU_525 nm

Appendix A3: Five Multispectral images of AA-URBC Sample.

AS1_375 nm

AS1_470 nm

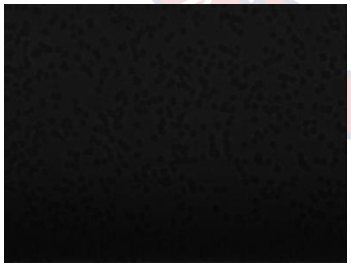

AS1_525 nm

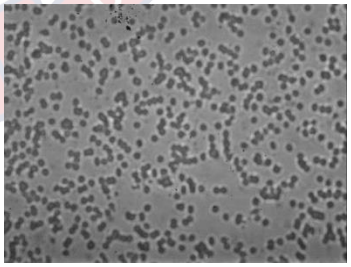

AS1_590 nm

AS1_625 nm

Appendix A4: Five Multispectral images of AS-IRBC-D1 Sample.

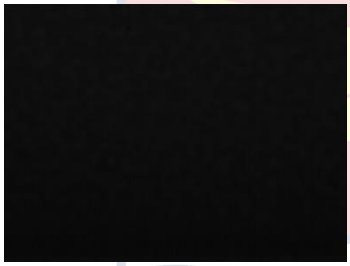

AS6_375 nm

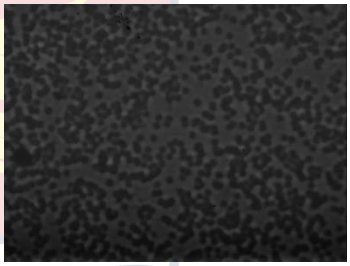

AS6_400 nm

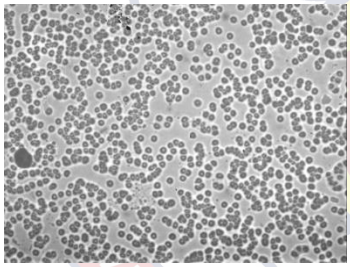

AS6_435 nm

AS6_525 nm

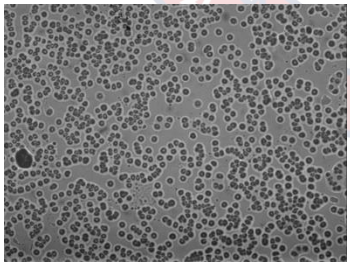

AS6_590 nm

Appendix A5: Five Multispectral images of AS-1RBC-D6 Sample.

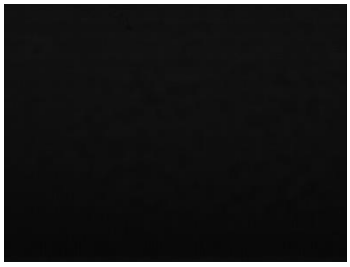

ASU_375 nm

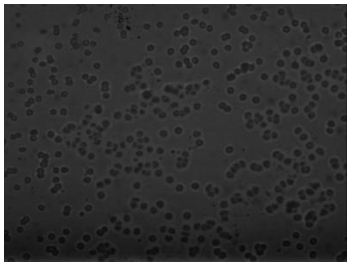

ASU_ 470 nm

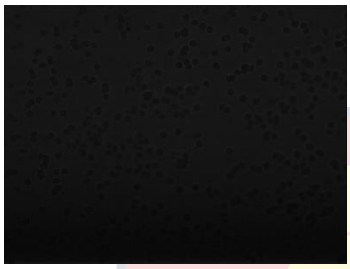

ASU_525 nm

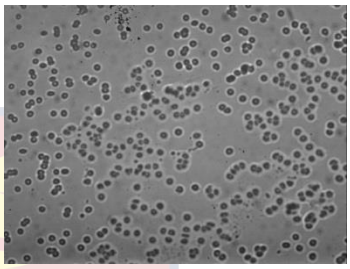

ASU_590 nm

ASU_625 nm

Appendix A6: Five Multispectral images of AS-URBC Sample.

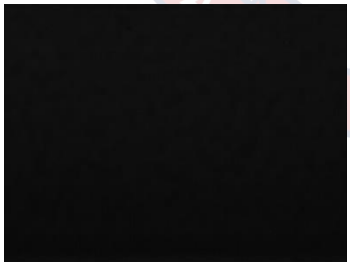

SS6_375 nm

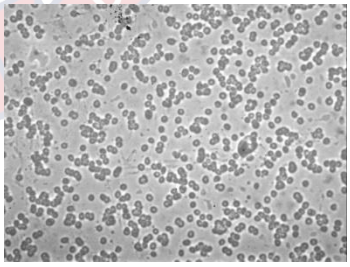

SS6_435 nm

SS6_470 nm

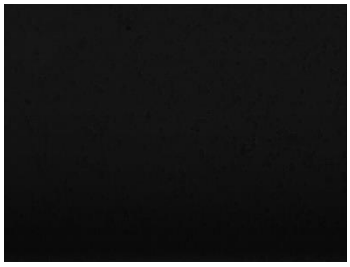

SS6_525 nm

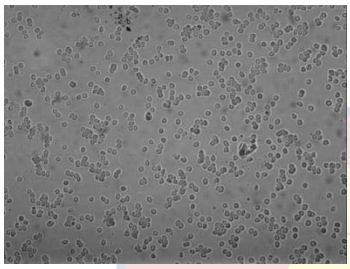

SS6_590 nm

Appendix A7: Five Multispectral images of SS-IRBC-D6 Sample.

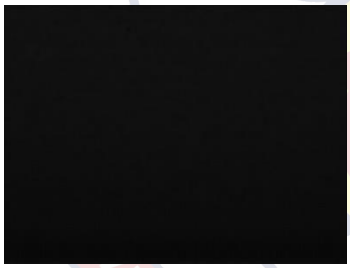

SSU_375 nm

SSU_400 nm

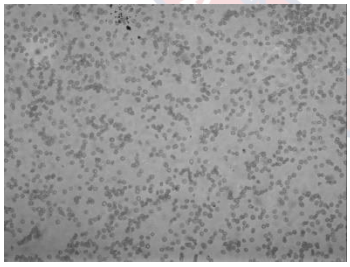

SSU_ 435 nm

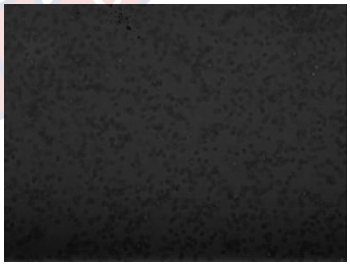

SSU_470 nm

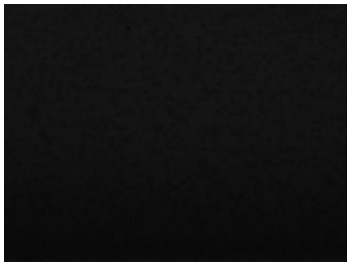

SSU_525 nm

Appendix A8: Five Multispectral images of SS-URBC Sample.

APPENDIX B: PHOTOGRAPH DEPICTING THE CULTURING OF *PLASMODIUM FALCIPARUM* PARASITE USING SICKLE RED BLOOD CELLS